1990-12

Free electron laser single-particle dynamics theory

Gillingham, David R.

Monterey, California: Naval Postgraduate School

NAVAL POSTGRADUATE SCHOOL
Monterey, California

THESIS

FREE ELECTRON LASER SINGLE-PARTICLE DYNAMICS THEORY

by

David R. Gillingham

December 1990

Thesis Advisor: W. B. Colson

REPORT DOCUMENTATION PAGE

Form Approved
OMB No 0704-0188

1a REPORT SECURITY CLASSIFICATION: UNCLASSIFIED	1b RESTRICTIVE MARKINGS
2a SECURITY CLASSIFICATION AUTHORITY	3 DISTRIBUTION/AVAILABILITY OF REPORT: Approved for public release; distribution is unlimited.
2b DECLASSIFICATION/DOWNGRADING SCHEDULE	
4 PERFORMING ORGANIZATION REPORT NUMBER(S)	5 MONITORING ORGANIZATION REPORT NUMBER(S)
6a NAME OF PERFORMING ORGANIZATION: Naval Postgraduate School; 6b OFFICE SYMBOL (If applicable): PH	7a NAME OF MONITORING ORGANIZATION: Naval Postgraduate School
6c ADDRESS (City, State, and ZIP Code): Monterey, CA 93943-5000	7b ADDRESS (City, State and ZIP Code): Monterey, CA 93943-5000
8a NAME OF FUNDING/SPONSORING ORGANIZATION; 8b OFFICE SYMBOL (If applicable)	9 PROCUREMENT INSTRUMENT IDENTIFICATION NUMBER
8c ADDRESS (City, State, and ZIP Code)	10 SOURCE OF FUNDING NUMBERS: PROGRAM ELEMENT NO; PROJECT NO; TASK NO; WORK UNIT ACCESSION NO

11 TITLE (Include Security Classification)
FREE ELECTRON LASER SINGLE-PARTICLE DYNAMICS THEORY

12 PERSONAL AUTHOR(S)
Gillingham, David, R.

13a TYPE OF REPORT	13b TIME COVERED	14 DATE OF REPORT (Year, Month, Day)	15 PAGE COUNT
Master's Thesis	FROM _____ TO _____	December 1990	63

16 SUPPLEMENTARY NOTATION The views expressed in this thesis are those of the author and do not reflect the official policy or position of the Department of Defense or the U. S. Government

17 COSATI CODES			18 SUBJECT TERMS (Continue on reverse if necessary and identify by block number)
FIELD	GROUP	SUB-GROUP	Free Electron Laser, Computer Simulation

19 ABSTRACT (Continue on reverse if necessary and identify by block number)

A detailed exploration of free electron laser (FEL) theory has been done in two areas. An exact solution to the phase-space trajectories in a linearly-polarized undulator has been obtained using a numerical simulation. The complicated phase-space motion caused by transverse undulator deflections makes a rigorous derivation for trajectories difficult, if not impossible. The numerical solution extends the understanding of electron trajectories by quantitatively describing the fast and slow components of motion. The Bessel function coupling coefficient,

20 DISTRIBUTION/AVAILABILITY OF ABSTRACT: ☒ UNCLASSIFIED/UNLIMITED ☐ SAME AS RPT ☐ DTIC USERS	21 ABSTRACT SECURITY CLASSIFICATION: Unclassified
22a NAME OF RESPONSIBLE INDIVIDUAL: W. B. Colson	22b TELEPHONE (Include Area Code): (408) 646-2765; 22c OFFICE SYMBOL: PH

DD Form 1473, JUN 86 *Previous editions are obsolete* SECURITY CLASSIFICATION OF THIS PAGE

S/N 0102-LF-014-6603 Unclassified

[19] Continued:

$J_o(\xi)-J_1(\xi)$, describing the slow evolution is found to be valid over a broad range of parameters even though its derivation is approximate.

A second program has been developed that provides a simple, quick diagnostic for accelerator designers to evaluate how well a simulated beam design will perform as an FEL. The effect of beam quality conditions like energy, angular, and positional spread are shown to depend only on the initial conditions of the beam at the entrance to the undulator. This program takes the six phase-space coordinates of the beam directly from an accelerator simulation code, like PARMELA, and predicts its performance in an FEL system. This method substitutes for more lengthy, complex integrated simulations, like INEX, that require a CRAY computer.

Approved for public release: distribution is unlimited.

FREE ELECTRON LASER SINGLE-PARTICLE DYNAMICS THEORY

by

D. R. Gillingham

Lieutenant, United States Navy

B. A., University of Colorado, 1983

Submitted in partial fulfillment of the

requirements for the degree of

MASTER OF SCIENCE IN PHYSICS

from the

NAVAL POSTGRADUATE SCHOOL

December 1990

Author: 

David R. Gillingham

Approved by: 

William B. Colson, Thesis Advisor

Xavier K. Maruyama, Second Reader

Karlheinz E. Woehler, Chairman,

Department of Physics

ABSTRACT

A detailed exploration of free electron laser (FEL) theory has been done in two areas. An exact solution to the phase-space trajectories in a linearly-polarized undulator has been obtained using a numerical simulation. The complicated phase-space motion caused by transverse undulator deflections makes a rigorous derivation for trajectories difficult, if not impossible. The numerical solution extends the understanding of electron trajectories by quantitatively describing the fast and slow components of motion. The Bessel function coupling coefficient, $J_o(\xi)-J_1(\xi)$, describing the slow evolution is found to be valid over a broad range of parameters even though its derivation is approximate.

A second program has been developed that provides a simple, quick diagnostic for accelerator designers to evaluate how well a simulated beam design will perform as an FEL. The effect of beam quality conditions like energy, angular, and positional spread are shown to depend only on the initial conditions of the beam at the entrance to the undulator. This program takes the six phase-space coordinates of the beam directly from an accelerator simulation code, like PARMELA, and predicts its performance in an FEL system. This method substitutes for more lengthy, complex integrated simulations, like INEX, that require a CRAY computer.

Table of Contents

ACKNOWLEDGEMENT

The author is grateful for support of this work by the Naval Postgraduate School, and the U. S. Office of Naval Research. The author would also like to thank W. B. Colson for his invaluable assistance and my wife Beth for her support.

I. INTRODUCTION

Since its conception in 1971, the free electron laser has been the subject of extensive theoretical and experimental work [Refs. 1-3]. While progress is being made on advanced designs, the fundamental theory of FELs is constantly being improved. There still remains many aspects of the basic theory which have not been solved exactly. The essential physics of the FEL is determined by the single-particle trajectories in the undulator and the evolution of the optical fields [Refs. 4,6]. Although FELs using linearly or circularly-polarized undulators work on the same principle, their electron phase-space trajectories are drastically different. The exact trajectories in a linearly-polarized undulator are complicated by motion coupled to the transverse undulator deflection which causes the longitudinal component of velocity to oscillate twice each undulator period. This causes difficulty in analysis, because these less-interesting, fast longitudinal oscillations cannot be precisely separated from the more-interesting, slow bunching motion responsible for gain. Historically, the fast motion has been averaged into a coupling coefficient which modifies the equation of motion for the slow evolution [Refs. 6-8]. A small error in the coupling coefficient could result in a large difference in the growth rate or ultimate power, especially in high-gain FELs.

It is important to consider the validity of the coupling coefficient used to describe the linearly-polarized undulator. The coupling coefficient uses $K[J_o(\xi)-J_1(\xi)]$, instead of just K for the helical case, where J_o and J_1 are Bessel functions of argument $\xi = K^2/2(1+K^2)$. $K = eB\lambda_o/2\pi mc^2$ is the undulator parameter, where e is the magnitude of the electron charge, B is the undulator rms field strength, λ_o is the undulator period, and mc^2 is the rest energy of the electron. The averaging method uses an approximation to the fast motion before taking a time-average over each period of the undulator. However, all derivations of the coupling

coefficient solve for the approximate fast motion without optical fields [Refs. 7-12]. This method is not completely rigorous, since the optical interaction is not included self-consistently. In order to make a more complete analysis, we derive the equation describing the z motion without approximation or assumption.

With the improvement of computer processing capabilities, the last ten years have seen the emergence of simulation as a necessary tool for some experiments. Projects that could cost millions of dollars are being evaluated for feasibility by simulations. As confidence improves, these methods are becoming more useful for designers. For FEL experiments, which are by nature, costly and complicated, the savings realized by simulation could be substantial. Programs like PARMELA, used at Los Alamos National Labs (LANL), are now used to design electron beam accelerators before projects are built. The ability to evaluate these designs as they perform as a system is essential. Integrated simulations like INEX currently perform this role, but as the accuracy improves, so does the size of the code, and therefore the time and money to run them. Another feature of such programs is the large amount of input required and prodigious output produced. Both serve to discourage casual use. A simple, quick diagnostic that accounts for the essential physics can fill the gap between accuracy and simplicity, and in turn serve as an accessible tool for the designer.

The effects of beam quality on the performance of the FEL can be predicted by the initial conditions of the beam at the entrance to the undulator. Electron accelerator simulations must keep track of the six phase-space coordinates of the sample electrons as they travel through the beam-line components. The output of the accelerator simulation can be used as the input for the FEL performance evaluator. The effects of off-axis undulator fields, which lead to betatron motion [Ref. 13], and either single or two-plane focusing are included to make the description complete [Ref. 14]. A simple equation that converts initial conditions into the meaningful FEL dimensionless phase-velocity is used to produce distributions

which describe the important parameters of FEL operation. This can also be made into a standard form for use with other previously developed models of beam quality effects.

II. BACKGROUND

A. FEL COMPONENTS

The complete FEL system consists of three major sections including the electron beam accelerator and transport section, the undulator, and the optical section, as illustrated in Figure 1. The accelerator section is the most complex section, and includes not only beam-line components, but auxiliary systems such as RF power and transport, vacuum systems, beam focusing and conditioning components, as well as shielding and diagnostic support. As an amplifier, the FEL magnifies a pre-existing light beam. In the amplifier configuration, the optics may consist of a seed laser and focusing elements. As an oscillator, the FEL starts from spontaneous emission, and builds up optical power until the losses equal the gain. In the oscillator configuration, the optics of a resonator cavity is made up of two or more mirrors, or may take on a variety of complex configurations. This thesis deals almost exclusively with the interaction inside the undulator, and assumes the electron beam is provided with the necessary parameters, and that the optical fields already exist in well-defined transverse and longitudinal modes.

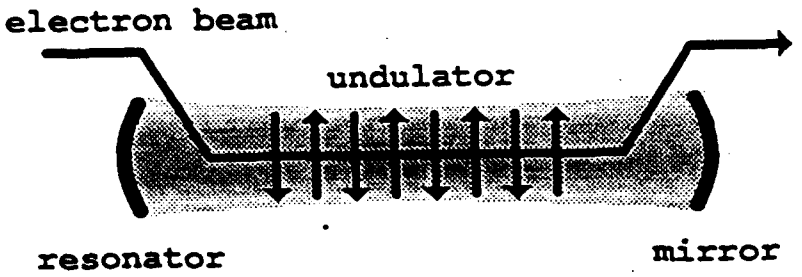

Figure 1. Elements of a typical FEL.

The transverse deflection of the highly relativistic electron beam in the alternating, periodic field of the undulator leads to classical spontaneous emission over a narrow spectrum and into a small forward cone about the longitudinal axis [Ref. 16]. Some of this radiation may be trapped inside the optical resonator, and provide the initial field for an oscillator. The interaction of the electrons with the combined fields of the light and undulator cause microscopic bunching on the scale of an optical wavelength. This microscopic bunching leads to coherent emission and optical gain [Ref. 17].

Beam quality must be sufficiently good to preclude degradation of the microscopic bunching either through energy or angular spread. A real energy spread causes the beam to "stretch out," because the individual electrons have different transit times through the undulator. If the energy spread is large enough to cause an axial spread in adjacent positions which is greater than an optical wavelength, then the gain mechanism will be adversely affected. A spread in the injection angle has a similar deleterious effect. The angular spread translates into a spread in longitudinal velocity as the individual electron velocities are projected onto the undulator axis. The effective mechanism is the same as for real energy spread and causes a longitudinal stretching that works against the microscopic bunching needed for gain.

The electron beam needed for FEL operation may take on a wide range of parameters depending on the use intended. Electron sources include induction linacs, RF linacs, electron storage-rings, Van de Graaffs, and microtrons, to name a few. Typically, the beam is provided as a series of RF pulses that vary in peak current from 1 A up to several kA. A direct current beam is less common and must operate at lower current because of power limitations, but may still be as high as 10 A. The beam radius may be from less than 1 mm up to 1 cm. The beam energy ranges from 1 MeV up to several GeV. Beam quality requirements depend on the specific FEL parameters for reasons discussed in the previous

paragraph. A more detailed discussion of the effect of beam quality to FEL performance is the subject of the last chapter of this thesis. Beam parameters can be tailored to suit the desired laser output quantities such as ultimate wavelength, and optical power, but because of the cost and complexity, beam parameters are essentially fixed after the initial design. The beam parameters must be combined with the specific undulator and optics parameters to complete the design of the laser.

The optical section for an oscillator usually consists of a resonator similar to standard laser designs. This may be a pair of spherical mirrors aligned axially, which sustain a transverse mode structure such as the fundamental Gaussian mode [Ref. 18]. A typical resonator length is about 5-10 m for an undulator that may be 1 to 3 m long. For optical wavelengths this represents a mode separation of $\lambda^2/2S \approx 0.001\,\mathring{A}$ for representative FEL parameters, where λ is the optical wavelength, and S is the resonator length. The gain bandwidth is substantially greater than this so it is not necessary to consider longitudinal boundary conditions. Resonator lengths must be chosen, for a given wavelength, in order to ensure that the fundamental transverse mode doesn't diverge too rapidly inside the undulator due to diffraction. This preserves a significant overlap between the transverse dimensions of the electron beam and the optical mode. Beam quality must also be constrained to prevent significant divergence for the same reason. Angular spread will cause the electron beam to diverge rapidly or limit the minimum spot size obtainable for focusing. Both effects limit the amount of transverse overlap between the electron beam and optical mode.

The undulator section is usually constructed of alternating magnetic pole pieces designed to present an intense, transverse, periodic field to the incoming highly relativistic electron beam. A typical peak field strength may be as high as a few Tesla, and have a period of a few cm. The relativistic contraction of the undulator period, as seen by the near light-speed electron beam, causes a Doppler

shift in the radiation, and is the mechanism that leads to short optical wavelength operation. Transverse fields may be constructed in a linearly-polarized structure, which leads to linearly-polarized light emission. As an alternative, the magnetic field may be circularly-polarized and can be made from helical electromagnetic windings [Ref. 19]. The helical windings have a higher peak field strength at shorter wavelength laser operation. Undulator construction is a field in itself, and has been the subject of much theoretical as well as experimental research. The theory for the helical undulator has the additional advantage that the mathematical analysis is simpler, and therefore is used as an example in many theoretical models. The important differences between helical and linear undulators is the major subject of Chapter III.

B. ELECTRON TRAJECTORIES INSIDE A HELICAL UNDULATOR

In order to discuss the principle of operation of the FEL, it is important to consider the individual electron trajectories inside the undulator without light. Typical electron beam sizes and currents are are in the Compton regime such that the electrostatic repulsion between the negatively charged electrons have a negligible effect. Furthermore, the beam is focused externally before entering the undulator. Under the influence of the undulator magnetic field, the electrons will deflect periodically from side to side, or "wiggle." The ideal form for the on-axis helical undulator field is

$$\vec{B}_m = B[\cos(k_o z), \sin(k_o z), 0] \quad , \tag{1}$$

were B is the peak undulator field strength, $k_o = 2\pi/\lambda_o$ is the undulator wave number associated with the period λ_o, and z is the distance along the longitudinal axis of the undulator. The Lorentz force law becomes

$$\vec{F} = \frac{d}{dt}(\gamma mc\vec{\beta}) = -e\vec{\beta}\times\vec{B}_m \quad , \quad \text{and} \quad \frac{d}{dt}(\gamma mc^2) = 0 \quad , \tag{2}$$

where $\gamma = 1/\sqrt{1-\beta^2}$ is the Lorentz factor, m is the rest mass of the electron, $e = |e|$

is the magnitude of the electron charge, $\vec{\beta} = \vec{v}/c$, and c is the speed of light. Let $\vec{\beta} = \vec{\beta}_{\parallel} + \vec{\beta}_{\perp}$, where the parallel component is along the axis of the undulator, and the perpendicular component refers to the transverse direction. Substituting the field in (1) into (2), and separating the components gives

$$\frac{d}{dt}(\gamma\beta) = \frac{e}{mc}\beta_{\parallel}B\,[\,-\sin(k_o z),\,\cos(k_o z),\,0] \quad , \quad \text{and} \quad \frac{d\gamma}{dt} = 0 \quad . \tag{3}$$

We see that the electron energy, γmc^2, and the parallel velocity, $\vec{\beta}_{\parallel}$, are constants of the motion. From conservation of energy, the magnitude of the transverse velocity $\beta_{\perp}$ must also be constant. The z motion can be written immediately as $z = \beta_{\parallel}ct$, where the entrance to the undulator is chosen to be at $z = 0$. Then, this can be substituted into the transverse equation, which can be integrated directly. The parallel component can be found through the coupling equation, $\gamma^{-2} = 1-\beta_{\parallel}^2 - \beta_{\perp}^2$. Assuming perfect injection, the exact velocity components can be written as

$$\vec{\beta}_{\perp}(t) = \frac{K}{\gamma}[\,\cos(\beta_{\parallel}k_o ct),\,\sin(\beta_{\parallel}k_o ct),\,\beta_{\parallel}] \quad , \quad \text{where} \tag{4a}$$

$$\beta_{\parallel} = \left[1-\frac{1+K^2}{\gamma^2}\right]^{1/2} \quad , \tag{4b}$$

and $K = eB\lambda_o/2\pi mc^2$ is the dimensionless undulator parameter for field strength B.

The maximum transverse deflection can be found by an additional integration and is

$$\vec{r}(t) = \frac{K\lambda_o}{2\pi\beta_{\parallel}\gamma}[\,\sin(\beta_{\parallel}k_o ct),\,-\cos(\beta_{\parallel}k_o ct),\,\beta_{\parallel}ct\,] \quad . \tag{5}$$

For typical FEL parameters, $K = 1$, $\lambda_o = 5$ cm, and $\gamma = 100$, this leads to an average deflection of $r = 0.1$ mm, which is smaller than the typical beam radius. Even if the deflections are too small to be visualized on the scale of the undulator, they still are responsible for significant spontaneous emission, and FEL gain.

The spontaneous emission mechanism is essentially classical, and can be described by the Larmor formula giving the total power emitted from a single electron as $P_e = 2e^2\gamma^4\dot{\beta}_\perp^2/3c$ (in cgs) [Ref. 16]. The transverse motion is already found, and the substitution gives $P_e = (8\pi r_e^2/3)(2\gamma^2 B_o^2 c/8\pi)$, where $r_e = e^2/mc^2$ is the classical electron radius. This radiation is narrowband and is emitted into a small cone about the forward axis of motion with approximate angular width $\approx \gamma^{-1}$. This radiation can be trapped in the optical resonator and used to supply the starting photons for oscillator operation. The interaction of these photons with the electron beam in the undulator is the essential concept of FEL physics. In the amplifier configuration, the photons are supplied by the seed laser.

C. ELECTRON INTERACTION WITH LIGHT

1. Description of Fields

The electron beam in the undulator with light present will be subject to the combined undulator and optical fields. Some time after startup, there will be a classical optical field in the sense that the wave's magnitude and phase can be measured with arbitrary precision. The optical fields are taken to be

$$\vec{E}_r = E[\cos(kz-\omega t+\phi), -\sin(kz-\omega t+\phi), 0] \quad , \quad \text{and} \tag{6a}$$

$$\vec{B}_r = E[\sin(kz-\omega t+\phi), \cos(kz-\omega t+\phi), 0] \quad , \tag{6b}$$

where E is the wave amplitude, $k = 2\pi/\lambda$ is the optical wave number for wavelength λ, $\omega = kc$ is the carrier frequency, and ϕ is the optical phase. In Figure 2, the net direction of the force, found by the vector relationship (2), on an electron depends on its location within a wavelength of light. Half the positions have a net force that retards their motion, and therefore lead to energy loss which is taken up in the optical field as the creation of photons. The remaining half of the positions gain energy from the optical field.

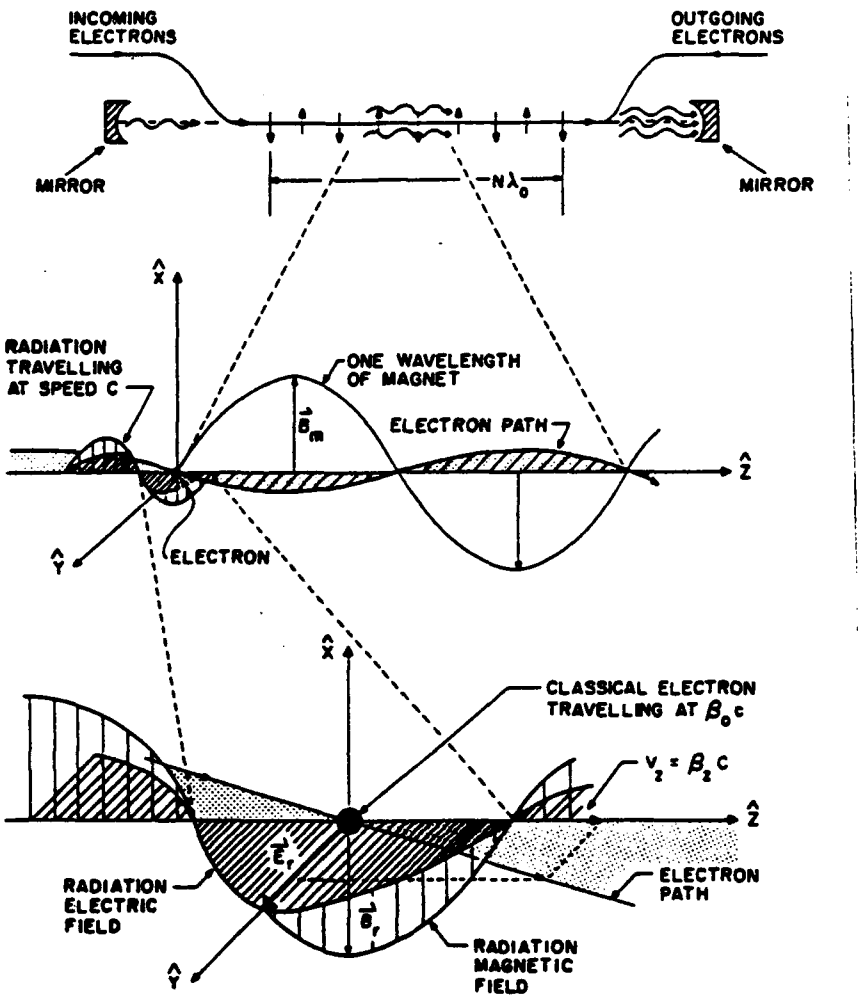

Figure 2. Vector diagram showing fields acting on the electron [Ref. 20].

Since the electron travels at slightly less than the speed of light, a number of optical wavelengths will pass over each electron as it travels the full length of the undulator. When exactly one optical wavelength passes over the electron in each undulator period resonance is established. Mathematically, this can be expressed by the condition

$$\beta_{\parallel} = \frac{k}{(k+k_o)} \quad . \tag{7}$$

Using the solution for $\beta_{\|} \approx 1-(1+K^2)/2\gamma^2$, for $\gamma \gg 1$, this can be inverted to find an expression for the resonant optical wavelength given a specific electron energy

$$\lambda = \lambda_o \frac{(1+K^2)}{2\gamma^2} \quad . \tag{8}$$

Unless specified otherwise, this equation will be used to discuss the resultant wavelength for FEL operation. In practice, given a specific electron energy, there are a number of factors which determine the ultimate optical wavelength, but it is roughly constrained to be in the vicinity of expression (8).

This relation also demonstrates some of the advantages of the FEL. Because factors like the electron beam energy, the undulator field strength, and the undulator period can be modified, the operating wavelength of the FEL can be tuned over a wide range. Also, because there is no internal medium other than electrons and co-propagating light, there is no physical limitation to the power density of the laser. Only external components, especially the optics tend to limit the power of operation. These are some of the most desirable features of the FEL.

2. The Wave Equation

Electrons that are close to one optical wavelength apart will experience identical forces. Therefore, a coordinate transformation that follows an electron with resonant velocity for the chosen wavelength is $\zeta = (k+k_o)z-\omega t$. This represents the phase of the electron within, roughly, one optical wavelength. The physical situation is identical over a period of $\Delta\zeta = 2\pi$. A phase velocity $\nu = L[(k+k_o)\beta_{\|}-k]$ describes how much faster or slower the electron is than its resonance velocity, where $\nu = 0$. In order to follow the growth of the optical field it is necessary to develop a wave equation. A classical wave equation may be written by summing the individual electron currents.

$$\Box^2 \vec{A} = -\frac{4\pi}{c}\vec{J} \quad ,$$

where $\Box^2 = \nabla^2 - \frac{1}{c^2}\frac{\partial^2}{\partial t^2}$ is the d'Alembertian operator, and $\vec{A}$ is the vector field potential, and $\vec{J}$ is the current density [Ref. 16]. An appropriate vector potential is $\vec{A} = (E/k)[\sin(kz-\omega t+\phi), \cos(kz-\omega t+\phi), 0]$. Assuming, the amplitude and phase vary slowly, and keeping only terms with single derivatives, the left hand side can be written as

$$\Box^2 A_\perp \simeq \left[\frac{\partial}{\partial z} + \frac{1}{c}\frac{\partial}{\partial t}\right] E e^{i\phi} \quad .$$

The total beam current can be represented as the sum of the single-particle currents $\vec{J}_i = -ec\vec{\beta}_i \delta^{(3)}(\vec{r}-\vec{r}_i)$, where $\vec{r}_i$ follows the trajectory of the i^{th} particle. Using the motion of the electron in the undulator field, the form for $\vec{\beta}_\perp$ can be inserted. Since the physical situation over one wavelength of light in Figure 2 is completely periodic, it is only necessary to sum over a period of λ. The result is [Ref. 17]

$$\mathring{a} = -j\langle e^{-i\zeta}\rangle \quad , \tag{9}$$

where the complex dimensionless field envelope and current are

$$a = \frac{4\pi NeKLEe^{i\phi}}{\gamma^2 mc^2} \quad , \quad j = \frac{8N(e\pi KL)^2\rho}{\gamma^3 mc^2} \quad , \tag{10}$$

E is the peak field strength, and ρ is the electron beam particle density. The open circle denotes a time derivative with respect to the dimensionless time variable, $\tau = ct/L$, and the brackets indicate a phase averaging over the sample electrons within a wavelength of light. If many electrons are uniformly spread in longitudinal position, then the phase average , $\langle e^{-i\zeta}\rangle$, will be zero, and there will be no optical field growth. In order to understand the FEL interaction, first it must be understood how electrons evolve from their initial positions within a wavelength of light.

3. The Pendulum Equation

To solve for the motion of electrons with light, again write the full equations of motion, the complete Lorentz force law is

$$\vec{F} = \frac{d}{dt}(\gamma mc\vec{\beta}) = -e[\vec{E} + (\vec{\beta}\times\vec{B})] \quad , \quad \text{and} \quad \frac{d}{dt}(\gamma mc^2) = -ec\vec{\beta}\cdot\vec{E} \quad .$$

Inserting the full combined fields of the undulator and optical fields, the transverse motion with perfect injection can be found again by direct integration.

$$\vec{\beta}_\perp = \frac{K}{\gamma}[\cos(k_o z), \sin(k_o z), 0] - \frac{A}{\gamma}[\sin(kz-\omega t+\phi), \cos(kz-\omega t+\phi), 0] \quad , \quad (11)$$

where $A = eE\lambda/2\pi mc^2$, analogous to the definition of K. The energy equation is

$$\frac{d\gamma}{dt} = \frac{-e}{mc}\vec{\beta}_\perp\cdot\vec{E} \quad (12)$$

The form for $\vec{\beta}_\perp$ can be inserted to yield the energy change equation,

$$\dot{\gamma} = \frac{\omega KA}{\gamma}\cos[(k_o+k)z-\omega t+\phi] \quad . \quad (13)$$

Using the relation $\gamma^{-2} = 1-\beta_\perp^2-\beta_\parallel^2$, an equation in the longitudinal variable $\beta_\parallel$ can be written. By rewriting the equation in terms of the dimensionless variable ζ, it can be shown that individual electrons follow motion described by a pendulum equation

$$\ddot{\zeta} = \dot{\nu} = |a|\cos(\zeta+\phi) \quad . \quad (14)$$

As electrons evolve along phase-space orbits, like a pendulum, they move in phase in such a way as to either drive or diminish the optical field through (9). Phases which make the argument of cosine between $-\pi/2$ and $\pi/2$ cause a gain in electron energy and a corresponding loss to the optical field. The other half of the possible phases lead to optical field growth. Using the pendulum equation it is possible to see by mathematical means what was said earlier: for a uniform distribution of initial phases, half the electrons gain energy and half lose. But, under the influence of the combined fields, the electrons evolve and can "bunch" at desirable phases and cause gain. The understanding of what leads to bunching of electrons

on the scale of an optical wavelength is the key to understanding the FEL. The combination of the pendulum equation and the wave equation form a complete description of the FEL, and can be simultaneously solved to show the effects of various initial conditions on operation.

Figure 3 shows the phase-space evolution of electrons in a helical undulator with light present, obtained by integrating (9) and (14) [Ref. 17]. The initial optical field is $a_o = 3$, and the initial phase-velocity is $\nu_o = 0$ (at resonance). The large picture shows the phase-space evolution of the sample electrons. The dots change in color from light to dark as they travel down the undulator. The dimensionless time variable runs from $\tau = 0 \rightarrow 1$. The sample electrons are initially chosen to be uniformly distributed in ζ. The solid line represents the separatrix which divides phase-space into closed and open orbits. The separatrix can be found by an elementary analysis of the pendulum equation.

Phase-space orbits can be found from the pendulum equation, (14), by integration. First, multiply both sides by 2ν to make it a perfect differential, so that

$$2\nu\dot{\nu} = 2|a|\dot{\zeta}\cos(\zeta) \quad ,$$

where the optical phase is neglected. This can be integrated to yield the equation of the phase-space orbits

$$\nu^2 - \nu_o^2 = 2|a|[\sin(\zeta) - \sin(\zeta_o)] \quad , \tag{15}$$

where ν_o and ζ_o are the initial phase-space coordinates. The separatrix corresponds to the phase-space path that passes through $\zeta_o = -\pi/2$, and $\nu_o = 0$. The resulting equation for the separatrix is

$$\nu_{sep} = \pm\sqrt{2|a|(\sin(\zeta)+1)} \quad , \tag{16}$$

which has a peak value of $\nu_{max} = \pm 2\sqrt{a_o}$. Points which start outside the region enclosed by the separatrix have "open" orbits, and points inside have "closed"

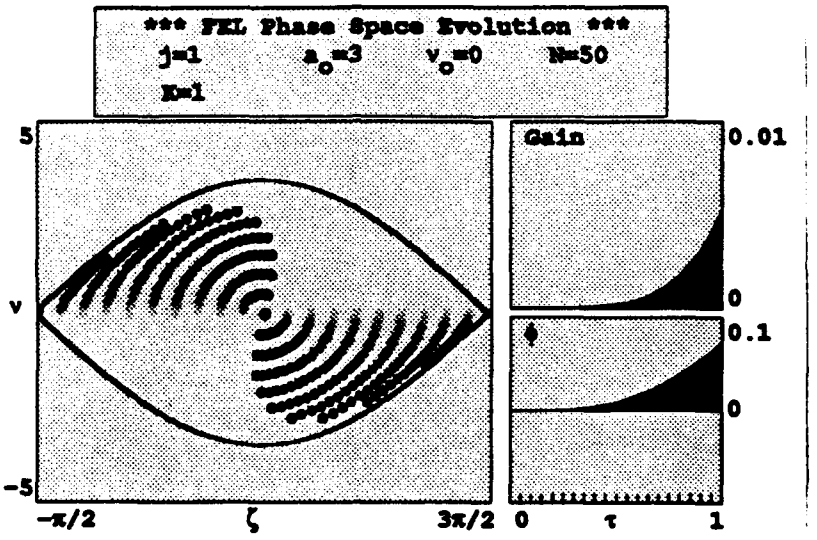

Figure 3. Phase-space evolution for monoenergetic electrons on resonance.

orbits. There are fixed points at $\zeta = -\pi/2$, $3\pi/2$, and $\pi/2$. The point at $\zeta = \pi/2$ is a stable fixed point which can be demonstrated by considering small deviations $\zeta = \pi/2+x$, where $x \ll \pi$. The substitution of this into the pendulum equation yields

$$\overset{\infty}{x} = |a|\cos(\pi/2+x) = |a|[\cos(\pi/2)\cos(x) - \sin(\pi/2)\sin(x)] = -|a|\sin(x) \quad .$$

Using the small angle approximation, $\sin(x) \approx x$, the equation becomes $\overset{\infty}{x} = -|a|x$ which gives simple harmonic motion which is stable. The points at $-\pi/2$ and $3\pi/2$ can be shown to be unstable [Ref. 21]. In Figure 3, all points start inside the separatrix, and therefore have closed orbits. Also displayed are the gain and phase evolution through the undulator. The gain and phase are found from solving the wave equation, (9).

Figure 4 shows the effect of starting above resonance. The electrons are started with $\nu_o = 2.6$, which corresponds to the maximum gain condition, which will be demonstrated below. Some electrons are trapped in closed orbits, and others are in open orbits. The open orbits move into the next wavelength, but wrap around because periodic boundary conditions are used. The gain is substantially higher and the optical phase change is less, because the electrons bunch near $\zeta = \pi$.

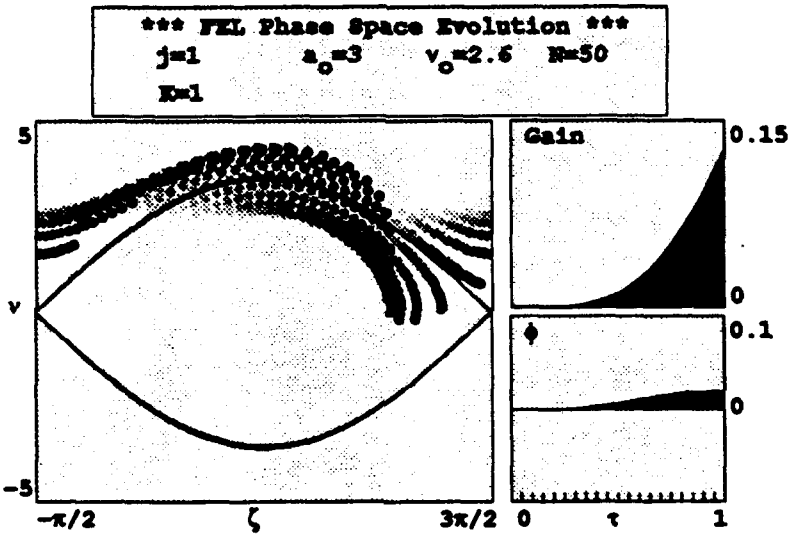

Figure 4. Phase-space evolution for monoenergetic electrons above resonance.

Assuming a uniform distribution in ζ, the small signal gain can be solved for, giving [Ref. 17]

$$G(\tau) = j\left[\frac{2 - 2\cos(\nu_o \tau) - \nu_o \tau \sin(\nu_o \tau)}{\nu_o^3}\right] .$$

Gain at the end of the undulator, $\tau = 1$, can be plotted as a function of ν_o for these

conditions, and is shown in Figure 5. This shows the maximum gain occurs at $\nu_o \approx 2.6$. The gain spectrum is anti-symmetric about $\nu_o = 0$, and is characteristic of small signal (low laser light intensity) and low gain FELs.

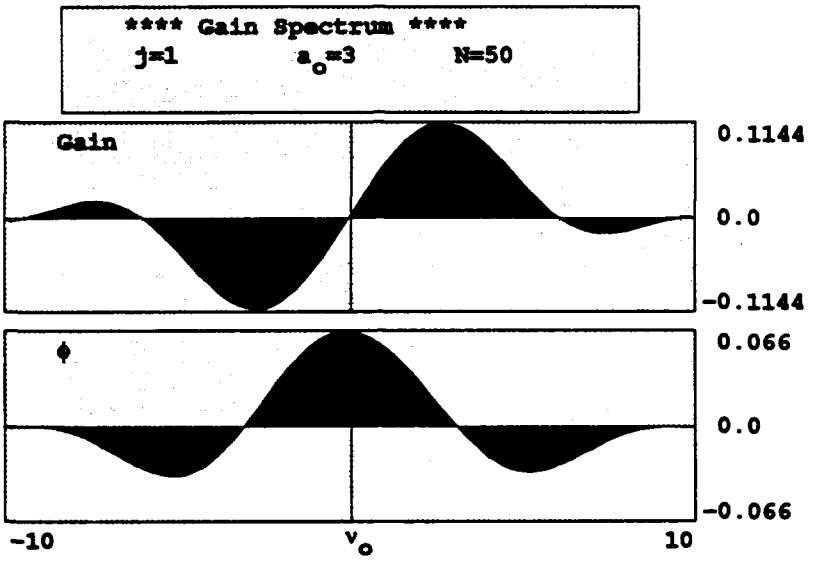

Figure 5. Small signal, low gain spectrum.

III. ELECTRON DYNAMICS IN A LINEARLY-POLARIZED UNDULATOR

A. MOTION WITH NO OPTICAL FIELD

1. Equations of Motion

The previous discussion is based on the helical undulator design. As stated earlier, there is an advantage in the analysis, because the motion is simpler. In this section, the exact motion in the linearly-polarized undulator is found. To construct a systematic approach, it is best to start with the motion of electrons in the presence of only the undulator field. The optical field will be considered later, after the method of approach has been established.

In the helical case with perfect injection, the electrons travel down the axis of the undulator with a constant velocity, $\beta_{\|}$. The transverse motion is constant in magnitude, but changes direction smoothly in a circular fashion. This makes the analysis simple, because the acceleration is constant in the equations, making it possible to solve a set of coupled differential equations. In the linear case, the acceleration is not constant, but varies as the electrons deflect from side-to-side in one transverse plane. This leads to difficulty in separating the equations of motion. In order to consider the motion, first consider an ideal linearly-polarized magnetic field on-axis

$$\vec{B}_m = B[\,0,\ \sin(k_o z),\ 0\,] \quad , \tag{17}$$

where B is the peak magnetic field. Since the magnetic field varies sinusoidally over each period, the rms value is $\bar{B} = B/\sqrt{2}$. Assign cartesian coordinates to the undulator with the origin at one end, the z axis along the longitudinal axis of the undulator, and the magnetic field in the y-plane. The electron motion will be in the

x-z plane. The equations of motion are

$$\frac{d}{dt}(\gamma\beta_x) = \beta_z \frac{eB}{mc}\sin(k_o z) \quad , \tag{18a}$$

$$\frac{d}{dt}(\gamma\beta_y) = 0 \quad , \tag{18b}$$

$$\frac{d}{dt}(\gamma\beta_z) = -\beta_x \frac{eB}{mc}\sin(k_o z) \quad , \quad \text{and} \tag{18c}$$

$$\frac{d}{dt}(\gamma) = 0 \quad . \tag{18d}$$

The x-component is a perfect derivative, and can be integrated directly to yield

$$\beta_x = -\frac{\sqrt{2}K}{\gamma}\cos(k_o z) \quad , \tag{19}$$

where $K = eB\lambda_o/2\pi mc^2$. In this case, perfect injection at $z = 0$ corresponds to the electron's x component of velocity at a maximum in the negative direction. The energy is a constant of the motion, neglecting losses to spontaneous emission, because the magnetic force acts at right angles to the electron's motion. Perfect injection also assumes that the other transverse component $\beta_y = 0$. Therefore, the perfectly injected beam must be sent into the undulator at an angle $\theta = \tan^{-1}(\beta_x/\beta_z) \approx \beta_x/\beta_z$. Since the longitudinal component $\beta_z \approx 1$, then $\theta \approx \sqrt{2}K/\gamma$. For typical values of FEL parameters, $K = 1$, $\gamma = 100$, so that $\theta \approx 0.01$ rad.

Substitution of the solution for β_x into the equation for β_z results in

$$\dot{\beta}_z = \frac{2K^2}{\gamma^2}k_o c\cos(k_o z)\sin(k_o z) \quad . \tag{20}$$

This can be made into a perfect differential by multiplying both sides by $2\beta_z$. Then,

$$\frac{d}{dt}(\beta_z^2) = -\frac{d}{dt}\left[2\frac{K^2}{\gamma^2}\cos^2(k_o z)\right] \quad , \quad \text{giving} \quad \beta_z^2 = -2\frac{K^2}{\gamma^2}\cos^2(k_o z) + C \tag{21}$$

where C is a constant of integration that accounts for initial conditions. At $z = 0$,

$\beta_{zo}^2 = 1-(1+2K^2)/\gamma^2$, so that $C = 1-\gamma^{-2}$. After some algebra, this can be separated into a form which can be integrated

$$\frac{dz}{\sqrt{\beta_{zo}^2 + (2K^2/\gamma^2)\sin^2(k_o z)}} = cdt \quad .$$

This can be integrated and the solution found in an inverted form, that is, with t as a function of z, as

$$t(z) = \frac{\lambda_o}{2\pi c\sqrt{\gamma^2-1}} F(\theta,M) \quad , \tag{22}$$

where $\theta = k_o z$, $M^2 = K^2/(\gamma^2-1)$, and F is an incomplete elliptic integral of the first kind.

2. Phase-Space Description

While this result is purely analytic, it is of restricted use, because $F(\theta,M)$ is a tabulated function. The actual trajectories will be evaluated later by numerical means. As discussed in the helical case, the important characteristic of the electron motion is bunching on an optical scale, and so the natural choice for description are the dimensionless phase-space variables, $\zeta = (k_o+k)z-\omega t$, and $\nu = L[(k_o+k)\beta_z-k]$. Although there is no light present, it is still possible to make the discussion in terms of the wavelength defined by the resonance condition (7). In the helical case, the electrons would appear as steady points in phase-space, (ζ,ν) that do not evolve. In the linear case, the side-to-side undulator deflection causes the electrons to orbit about these steady points at twice the undulator periodicity. To illustrate this, first write the complete expression for the longitudinal velocity

$$\beta_z(z) = \sqrt{\beta_{zo}^2 + (2K^2/\gamma^2)\sin^2(k_o z)} \quad . \tag{23}$$

In the regime where $(K/\gamma)^2 \ll 1$, this can be approximated by a binomial expansion.

$$\beta_z(z) \approx \beta_{zo} + \frac{K^2}{\gamma^2}\sin^2(k_o z) \quad . \tag{24}$$

Over the full range of possible arguments for z, β_z varies by $\Delta\beta_z \approx \pm K^2/2\gamma^2$. This will cause a variation in phase velocity v by $\Delta v = \pm L(k+k_o)\Delta\beta_z \approx 2\pi N K^2/(1+K^2)$. For a typical value of K=1, and N=50, this means a variation of $\Delta v \approx \pm 50\pi$ during each half period of the undulator. This is 50 times greater than the natural gain bandwidth of 2π!

The extent of motion in ζ cannot be computed without an approximate solution of the elliptical equation. A perturbation in powers of $(K/\gamma)^2$ to first order will suffice. The result is

$$z(t) \approx \bar{\beta}_z ct + \frac{\lambda_o K^2}{8\pi\gamma^2}\cos(2\bar{\beta}_z k_o ct) + \cdots \quad , \tag{25}$$

where $\bar{\beta}_z$ is the average value over a half-period. This can be computed analytically by the results above, and is

$$\bar{\beta}_z = \frac{\pi\sqrt{\gamma^2-1}}{2F(\pi/2, M)} \approx \beta_{zo} + \frac{K^2}{2\gamma^2} \quad . \tag{26}$$

This results in a variation of $\Delta z \approx \pm\lambda_o K^2/2\pi\gamma^2$.

$\zeta(t)$ can be computed directly as

$$\zeta(t) = (k+k_o)z(t) - \omega t \approx \bar{\zeta}(t) + \xi\cos(2\omega_o t) \quad , \tag{27}$$

where $\bar{\zeta}(t) = (k+k_o)\bar{\beta}_z ct - \omega t$, $\xi = K^2/2(1+K^2)$, and $\omega_o = \bar{\beta}_z k_o c$. The variation in ζ is $\Delta\zeta = (k+k_o)\Delta z \approx \pm K^2/2(1+K^2)$. For a typical design with $K = 1$, $\Delta\zeta \approx \pm 1/4$. For the periodicity of 2π in ζ, this variation has a width of $\pi/6$. This is still only a fraction of a wavelength, so it is not expected to destroy the microscopic bunching mechanism needed for gain. But, $\Delta\zeta$ is responsible for harmonics.

A numerical solution to the phase-space motion of electrons in a linearly-polarized undulator is shown in Figure 6. The FEL parameters used are $N = 50$, $\lambda = 5$ cm, $\gamma = 100$, $K = 1$, $j = 0$ (not needed unless light present), and a_o very small

(no light). Periodic boundary conditions have been used again. The motion is symmetric, and the variations agree with the approximate values computed above.

Although the sampled electrons are equally spaced on the average, in Figure 6 they are not actually equally spaced longitudinally as they travel through the undulator. The electrons are at different phases in their elliptical orbits compared to adjacent electrons. These differences are obscured by the periodic nature of the orbits, however, it can be observed by watching the simulation as it runs. The transverse deflection slows them down, and they tend to bunch as they reach their maximum deflection. They spread out again as they move back to the axis. This "artificial" bunching, in the sense that it does not come from the optical fields, requires some care in selecting the electron's initial conditions. It does not suffice to take a uniform distribution as a starting point. The electrons must be presented to the undulator one at a time, just as it occurs in the real beam. This requires an extreme amount of precision until all the sample electrons are in place, then the simulation can proceed as usual. Failure to provide for this effect can lead to a non-physical pre-bunching which would create false gain. Also, it was found that great care needed to be taken in the calculations, because of the fine scales involved, which were on the order of one part in a million. Although the electrons move above and below resonance by large amounts, they must return to the exact same conditions after each half-period of the undulator. In practice, to calculate this requires double precision throughout, and a fourth-order Runge-Kutta-Nystrom integration technique [Ref. 23].

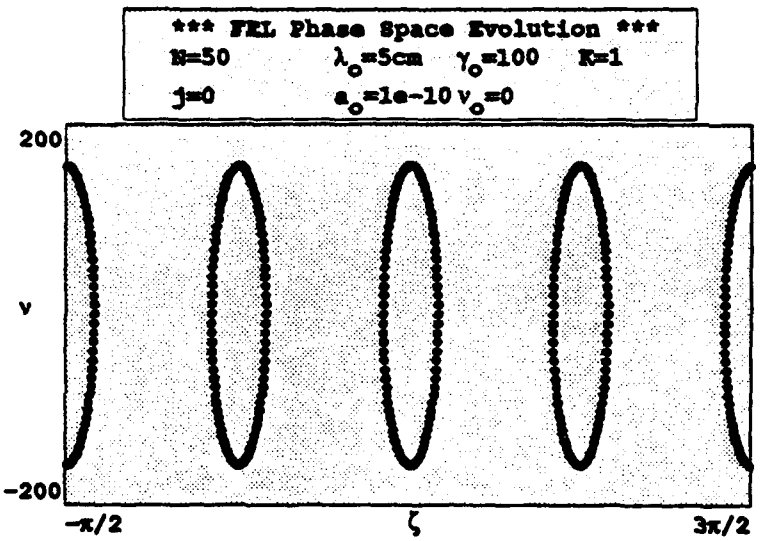

Figure 6. Exact phase-space trajectories of electrons in a linearly-polarized undulator with no light present. The optical wavelength is determined by the resonance condition.

B. MOTION IN THE PRESENCE OF OPTICAL FIELDS

1. Derivation of the Exact Equations of Motion in Ideal Fieldsj

Assume now that there is an actual optical field present, due either to a seed laser (amplifier), or by captured spontaneous emission (oscillator). In the case of the oscillator, with the assumption of plane-waves, the fields must have the same polarization as the motion of the electron. The far-field radiation will be due solely to the acceleration fields, in which case, the electric field vector will be in the same plane as the electron's motion, and the magnetic field at right angles to it. Fields that meet all of these requirements are

$$\vec{E}_R = E[\cos(kz-\omega t+\phi), 0, 0] \quad \text{and} \quad \vec{B}_R = E[0, \cos(kz-\omega t+\phi), 0] \quad , \tag{28}$$

where E is the electric field magnitude, $k = 2\pi/\lambda$ is the optical wavenumber for wavelength λ, ω is the carrier frequency, and ϕ is the optical phase. The equations of motion are

$$\frac{d}{dt}(\gamma mc\,\beta_x) = -eE\cos(kz-\omega t+\phi) + e\beta_z[B\sin(k_o) + E\cos(kz-\omega t+\phi)] \quad , \tag{29a}$$

$$\frac{d}{dt}(\gamma mc\,\beta_y) = 0 \quad , \tag{29b}$$

$$\frac{d}{dt}(\gamma mc\,\beta_z) = -e\beta_x[B\sin(k_o z) + E\cos(kz-\omega t+\phi)] \quad , \quad \text{and} \tag{29c}$$

$$\frac{d}{dt}(\gamma mc) = -e\beta_x E\cos(kz-\omega t+\phi) \quad . \tag{29d}$$

The transverse x-component equation can be written as

$$\frac{d}{dt}(\gamma\beta_x) = \sqrt{2}A\cos(\psi)\dot{\psi} + \sqrt{2}K\sin(\theta)\dot{\theta} \quad , \tag{30}$$

where $K = eB\lambda_o/2\pi mc^2$, $A = eE\lambda/2\pi mc^2$, $\theta = k_o z$, $\dot{\theta} = k_o \dot{z}$, $\psi = kz-\omega t+\phi$, and $\dot{\psi} = k\dot{z}-\omega$. Note that the time derivative of the optical phase is ignored, because low gain is assumed. (30) is a perfect derivative, and can be integrated directly to give

$$\beta_x = -\sqrt{2}\frac{K}{\gamma}\cos(\theta) + \sqrt{2}\frac{A}{\gamma}\sin(\psi) \quad , \tag{31}$$

where perfect injection has been assumed. This allows an exact expression for the energy change to be found as

$$\dot{\gamma} = \frac{2\omega}{\gamma}\left[KA\cos(\theta)\cos(\psi) - A^2\sin(\psi)\cos(\psi)\right] \quad . \tag{32}$$

These two equations, (31) and (32), along with $\gamma^{-2} = 1-\beta_z^2-\beta_x^2$, are sufficient to find a differential equation for the z-component. After some rearrangement, the equation reads

$$\frac{\dot{\beta}_z}{1-\beta_z^2}=\frac{\omega A^2(\beta_z-1)\sin(2\psi)+KAf_-(\beta_z)\cos(\theta+\psi)-KAf_+(\beta_z)\cos(\theta-\psi)+\omega_o K^2\sin(2\theta)}{1+2K^2\cos^2(\theta)-4KA\cos(\theta)\sin(\psi)+2A^2\sin^2(\psi)} \quad (33)$$

where $\omega_o = k_o c$ and $f_\pm = \omega_o \pm \omega(\beta_z - 1)$. Without light, $A=0$, this reduces to the equation of motion with the undulator fields alone, (20), and leads to the elliptic functions previously derived. The complete equation as it appears cannot be solved analytically. As an approximation, (33) can be shown to reduce to the pendulum equation in the regime where K/γ is small.

2. Pendulum Equation for the Linearly-Polarized FEL

In the equation for the energy change $\dot{\gamma}$, consider the term A^2 compared to KA. The value of A depends on the optical field, a, which is limited by saturation. The strongest optical field forces the electrons into about one synchrotron oscillation during their pass through the undulator. Synchrotron motion is the periodic oscillation in the longitudinal direction as compared to betatron motion which is in the transverse direction.

The analysis of the phase-space motion shows that there is a stable fixed point at $\zeta = \pi/2$. The electrons in closed orbits follow nearly circular paths about the stable fixed point. Examine small deviations $\zeta = \pi/2+x$, where $x \ll \pi$. Substitution of this form into the pendulum equation yields $\ddot{x} = |a|\cos(\pi/2+x)$. Use the trigonometric identity $\cos(\pi/2+x) = \cos(\pi/2)\cos(x)-\sin(\pi/2)\sin(x) \approx -x$. This gives a harmonic equation $\ddot{x} = -|a|x = -\nu_s^2 x$, where $\nu_s = \sqrt{|a|}$ is the dimensionless synchrotron frequency. The assumption of approximately one synchrotron oscillation during a pass through the undulator implies that $\nu_s = 2\pi \Rightarrow |a| \approx 4\pi^2$.

If this estimate for strong fields is substituted into the definition of $|a|$, then

$$|a|_{sat} = \frac{8\pi^2 KLNA}{\gamma^2\lambda} \approx 4\pi^2 \quad . \quad (34)$$

Using the resonance equation $\lambda = \lambda_o(1+K^2)/2\gamma^2$, we find that

$$\frac{A}{K} \approx \frac{1}{4N^2}\frac{(1+K^2)}{K^2} \quad . \tag{35}$$

For $K=1$, $A/K \approx 1/2N^2$, so that even for a small number of periods, say, $N \gg 10$, the ratio of terms is limited to $A/K < 1/200$. For more conventional designs, the ratio is even smaller yet, and therefore, the effect of neglecting the A^2 term is minimal.

It is now possible to write the approximate energy equation as

$$\dot{\gamma} \approx \frac{2\omega}{\gamma} AK\cos(\theta)\cos(\psi) \quad . \tag{36}$$

By use of a trigonometric identity [Ref. 23], it can be rewritten in a way which separates the fast and slowly evolving terms

$$\dot{\gamma} = \frac{\omega}{\gamma} AK[\cos(\psi+\theta) + \cos(\psi-\theta)] \quad . \tag{37}$$

The arguments can be rewritten as

$$\psi+\theta = (k+k_o)z(t)-\omega t = \zeta(t) \quad \text{and} \quad \psi-\theta = (k+k_o)z(t)-\omega t-2k_o t = \zeta(t)-2\theta \quad .$$

From (27), $\psi+\theta \approx \bar{\zeta}(t)+\xi\cos(2\theta)$, and $\psi-\theta \approx \bar{\zeta}(t)+\xi\cos(2\theta)-2\theta$. The cosine terms can be expanded into products of slowly-varying and fast-varying terms by applying another trigonometric identity so that

$$\cos(\psi+\theta) \approx \cos(\bar{\zeta})\cos(\xi\cos(2\theta)) - \sin(\bar{\zeta})\sin(\xi\cos(2\theta) \quad , \quad \text{and}$$

$$\cos(\psi-\theta) \approx \cos(\bar{\zeta})\cos(2\theta-\xi\cos(2\theta)) + \sin(\bar{\zeta})\sin(2\theta-\xi\cos(2\theta)) \quad .$$

These terms can be averaged over a period of the undulator, assuming that $\bar{\zeta}$ varies slowly and its value remains essentially constant over one period. Over one period, the argument θ varies from 0 to 2π. For an arbitrary function of θ, the average value over one undulator period is

$$\langle g(\theta)\rangle = \frac{1}{2\pi}\int_0^{2\pi} g(\theta)d\theta \quad .$$

The average energy change rate then can be evaluated directly from the following integrals [Ref. 23]:

$$\frac{1}{2\pi}\int_0^{2\pi}\cos(\xi\cos(2\theta))d\theta = J_o(\xi) \quad , \tag{38a}$$

$$\frac{1}{2\pi}\int_0^{2\pi}\cos(2\theta-\xi\cos(2\theta))d\theta = -J_1(\xi) \quad , \tag{38b}$$

$$\frac{1}{2\pi}\int_0^{2\pi}\sin(\xi\cos(2\theta))d\theta = 0 \quad , \quad \text{and} \tag{38c}$$

$$\frac{1}{2\pi}\int_0^{2\pi}\sin(2\theta-\xi\cos(2\theta))d\theta = 0 \quad , \tag{38d}$$

where J_o and J_1 are zeroth and first-order ordinary Bessel functions. Substitution of these integrals into the averaged energy rate of change equation gives the following result [Ref. 6]

$$<\dot{\gamma}> = \frac{\omega}{\gamma}AK[J_o(\xi)-J_1(\xi)]\cos(\zeta+\phi) \quad . \tag{39}$$

This differs from the helical case only in the replacement of K by $K[J_o(\xi)-J_1(\xi)]$. The argument ξ varies from zero up to maximum value of 1/2. The Bessel function coefficient therefore varies from a value of 1 at $K=0$, down to 0.72 as $K\to\infty$. This can be carried through everywhere K appears, and therefore, it is the only modification necessary to derive the pendulum equation for the linearly-polarized undulator. The slowly-evolving phase-space motion in the linearly-polarized undulator is then

$$\overset{oo}{\zeta} = |a|\cos(\zeta+\phi) \quad , \tag{40}$$

where $|a| = 4\pi NeK[J_o(\xi)-J_1(\xi)]LE/\gamma^2 mc^2$. All of the previous results from the phase-space evolution in the helical undulator can be used to describe the linearly-polarized undulator.

While, this result is essentially correct in the regime where K/γ is small, this "standard" derivation has a number of mathematical problems. Namely, a number of factors were assumed to be essentially constant over one period of the undulator. Secondly, approximate solutions to the z motion are used from the

"no-light" solution obtained in the earlier section. This cannot be complete because the effect of the light on the motion is neglected. This is not a rigorous perturbation scheme, because the end result contains all powers of the optical field in the trigonometric argument in ζ. Other derivations proceed along the same lines, and while more sophisticated, suffer from the same inconsistency. For this reason, it is important to return to the exact differential equation (33), and seek an alternative means of solution. A way of accomplishing this with a minimum of difficulty is numerical simulation. Since (33) cannot be solved rigorously, not only is numerical simulation easier, it is more appropriate and can extend the solution into regimes where the $K/\gamma \ll 1$ condition is not met.

C. NUMERICAL SOLUTION TO THE EXACT EQUATIONS OF MOTION

1. Time-Averaged Phase-Space Trajectories

Equation (33) can be solved exactly by numerical means. This, however, is not a complete description of an FEL because the field evolution must also be included. Because of this necessity, the solution shall be restricted to the low gain case such that the optical field evolution can be described by the slowly-varying wave equation (9), and where the time derivative of the optical phase ϕ can be ignored in the Lorentz force equation. There are, however, no restrictions on the values of K and γ. The exact motion can be found by integrating (33), and displaying the results in the traditional phase-space description (ζ,ν), which was developed earlier.

Figure 7 illustrates the phase-space motion of a single electron in the presence of an optical field. The FEL parameters used are chosen to be illustrative, and do not represent a specific FEL design. In particular, the number of periods, $N = 3$, is chosen to limit the number of "loops" in the picture so that the motion would be clear. The optical field, $|a| = 3$, is below saturation, and large

enough to cause noticeable motion. The current, $j = 1$, was chosen to be in the low gain regime, so that the model conditions would be met. The motion demonstrates the same fast oscillation previously described. The point about which the electron oscillates, however, evolves in a manner similar to the the way the electrons in the helical undulator did in the presence of optical fields. This suggests a reasonable means for comparison of the numerical solution to the approximate analytical result that led to a modified pendulum equation (40). If the center point of the fast oscillations can be followed, then the equation of motion of the center should resemble the solution to the pendulum equation. This can provide a validation of the approximate results, and of the Bessel function coupling coefficient, $J_o(\xi)-J_1(\xi)$.

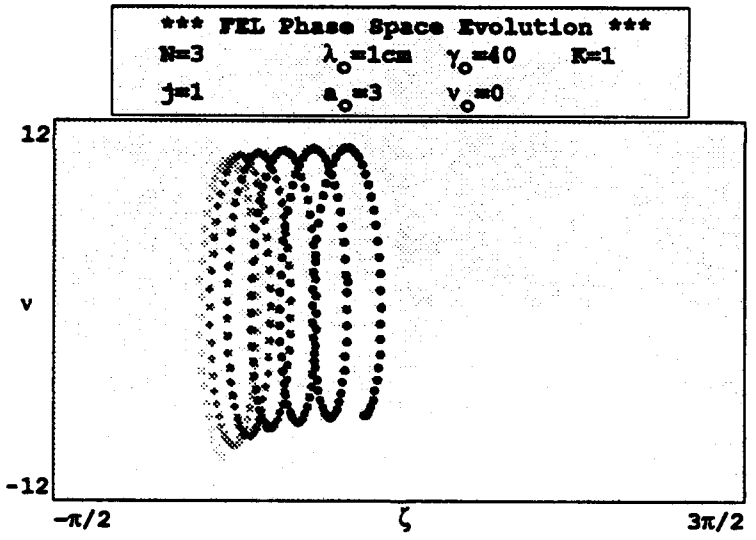

Figure 7. Exact numerical solution to motion with light present.

The center of the fast oscillations can be determined by the time-averaged phase-space coordinates over each period of the fast motion. The fast motion is caused by undulator deflection, so that the fast oscillation has a period of exactly

half the undulator period. This period can be found exactly, because the average longitudinal velocity without light is known exactly, either from (26) or determined numerically. Figure 8 shows the results of half-period averaging of the exact phase-space motion with light present. As can be seen easily, the averaged motion follows the exact evolution. The fast motion doesn't need to be followed within each period, because the optical fields evolve slowly over several periods. The phase-space trajectories do not depend on the fast motion, but the averaged, slowly-evolving motion. Therefore the fast motion is less-interesting, but has the undesired property that it covers a much greater scale than the slow motion. There is no loss of generality in following, but omitting to display, the fast motion. The optical fields depend only on the slow motion which can be put into the wave equation (9). Figure 9 shows the same situation as Figure 8, but omits the fast display.

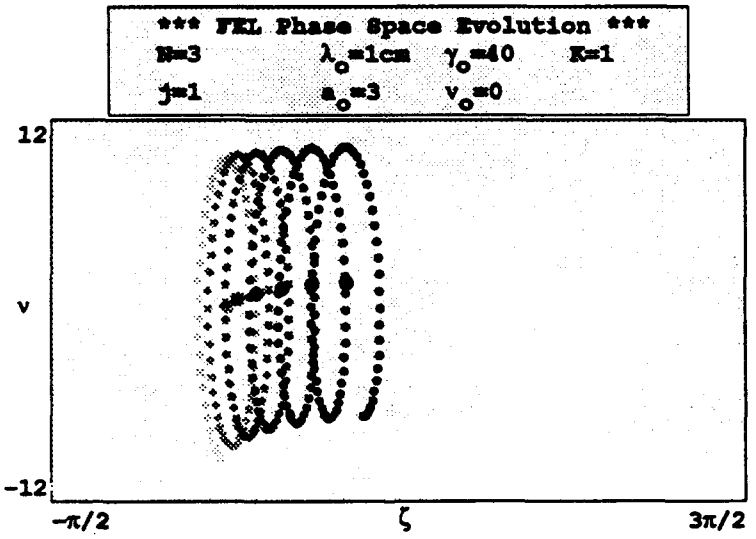

Figure 8. Exact fast motion and slow time-averaged motion.

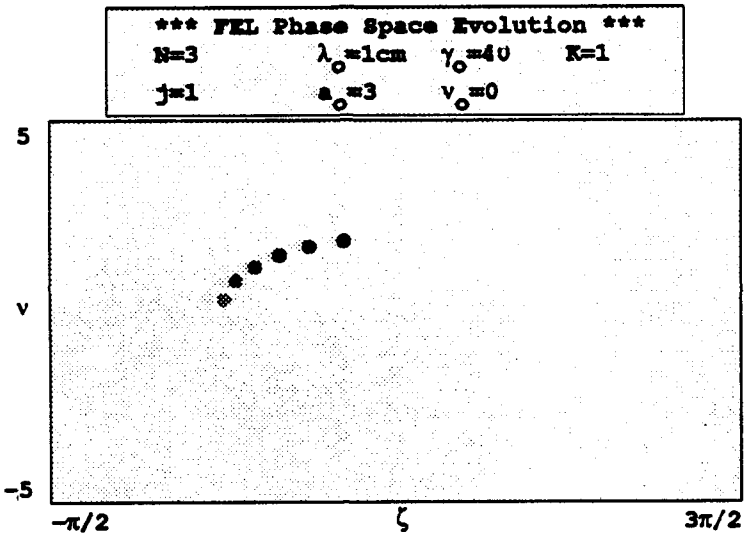

Figure 9. Slow time-averaged motion with fast oscillation omitted.

2. Comparison with the Modified Pendulum Equation

It is now possible to use this method to solve for the evolution of a uniform distribution sampling of electrons in phase, and use the results to follow their evolution in phase-space. Figure 10 shows the case with twenty sample electrons, which are equally spaced in time as they enter the undulator, and are at the exact resonance energy. As it appears, they follow trajectories that could be described by solving the pendulum equation.

This can be compared directly to the numerical solution of the pendulum equation in Figure 11 directly below it. The motion has the same general features, but does not have the same amplitude. The Bessel function coupling coefficient can account for the difference. For this case, $K = 1$, the argument of the Bessel functions, $\xi = K^2/2(1+K^2) = 1/4$. This yields as factor $J_o(\xi)-J_1(\xi) = 0.86$. This

factor modifies two parameters: the optical field, a_o, and the current j. With the substitutions, $a \rightarrow a[J_o(\xi)-J_1(\xi)]$ and $j \rightarrow j[J_o(\xi)-J_1(\xi)]^2$, the new parameters become $a_o = 2.6$, and $j = 0.71$. Figure 12 is the numerical solution of the pendulum equation using the Bessel function coupling coefficient modifications. The motion is now virtually indistinguishable from the exact solution in Figure 10. For these parameters, the Bessel function coupling coefficient modification to the pendulum equation is an accurate model to the exact time-averaged phase-space motion in the linearly-polarized undulator.

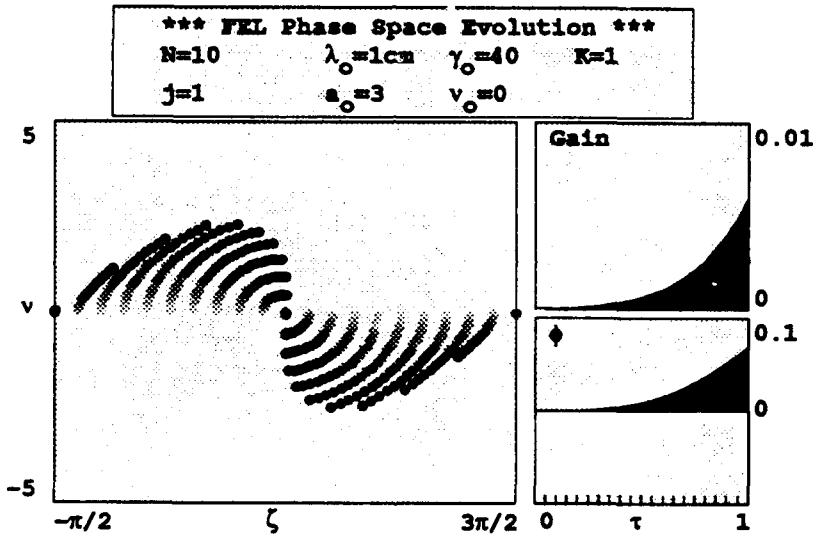

Figure 10. Exact time-average numerical solution for linear undulator with electrons exactly on resonance, and uniform longitudinal distribution.

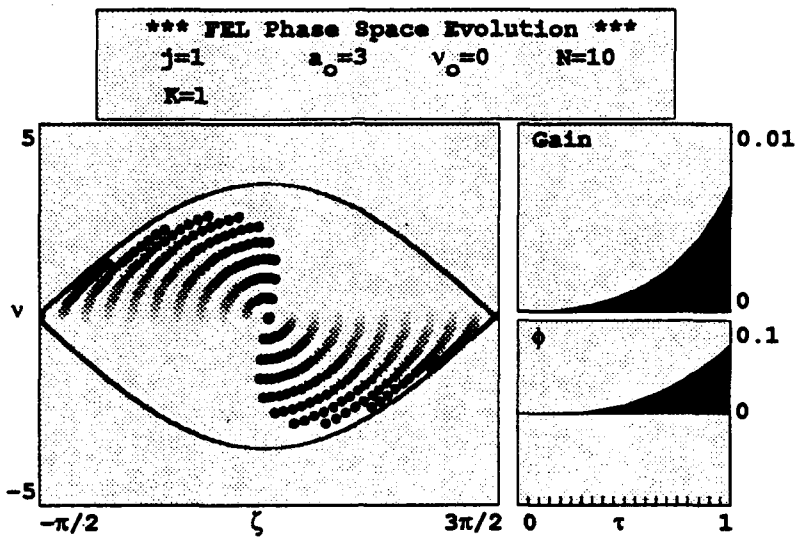

Figure 11. Numerical solution to the pendulum equation with identical FEL parameters.

3. Range of Validity for $J_0(\xi)-J_1(\xi)$

Although the success of modeling the time-averaged exact motion with the Bessel function coupling coefficient modification to the pendulum equation is encouraging, it has only been demonstrated in a regime where K/γ is small. This, however, was precisely where the approximate analytical solution could be found. Now the question arises, what is the range of validity for the approximate result? Previously, there have been few means available to answer this question. The numerical solution of (33) with time-averaging provides a visual means for comparison. Just like what was done previously, different values of K/γ can be used, and compared to the numerical solution of the Bessel function coupling coefficient modified pendulum equation. If the motion is identical, then the results are compatible.

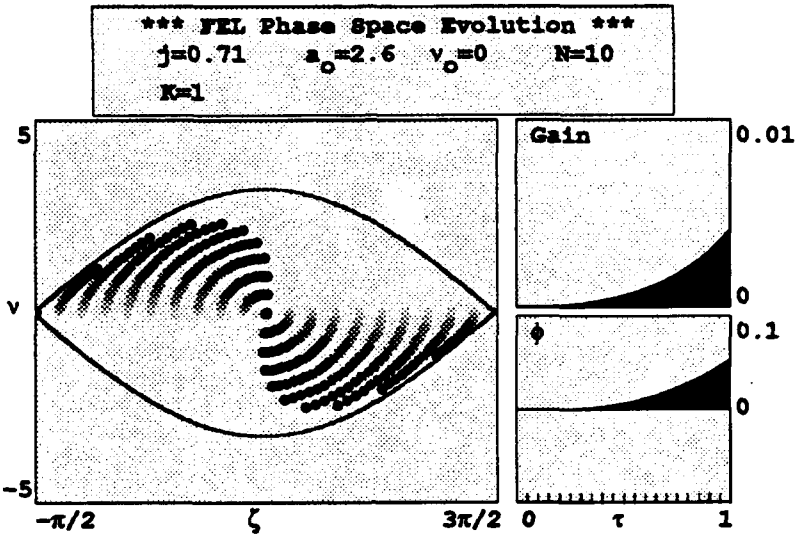

Figure 12. Numerical solution to the pendulum equation with Bessel function coupling coefficient modifications to a_o and j.

However, K/γ cannot be chosen to be arbitrarily large. The physical significance of K/γ can be seen from the previous results with no light present. The larger the magnetic field, the larger is the transverse deflection of the beam in the undulator. This in turn reduces the longitudinal component of velocity. At the most extreme, the deflection can completely turn the beam around, and no electrons will pass through the undulator. If γ in turn is made larger, the beam will still have enough energy to make it past the undulator deflection. A limiting case can be found by setting $\beta_{zo} = 1-(1+2K^2)/\gamma^2 = 0$. For a given value of K, the minimum energy needed to make it through the undulator is $\gamma_{min}^2 = 2K^2+1$. For an example of $K = 1$, this leads to $\gamma_{min} = \sqrt{3}$, and $K/\gamma = 1/\sqrt{3} \approx 0.58$.

At low energies that are above γ_{min}, the resulting deflection may cause the beam to transition from the relativistic regime. In phase-space, this will cause

some degree of asymmetry. In Figure 13, $K = 1$ and $\gamma = 2$, and the optical field is $a_o = 0$. The resulting orbits without any light present are highly asymmetric because β_z varies at the top and bottom. This suggests that this regime may be in clear violation of some of the assumptions used in the standard derivation of (40). The electron's velocity in the z direction can not be treated as a constant with value $\beta_z \leq 1$. The precise variation of β_z must be included, making it even more difficult to obtain simple integral relations that lead to the Bessel function coupling coefficients. An exact result is impossible, not only in practice, but for reasons discussed earlier, the method cannot be considered strictly rigorous.

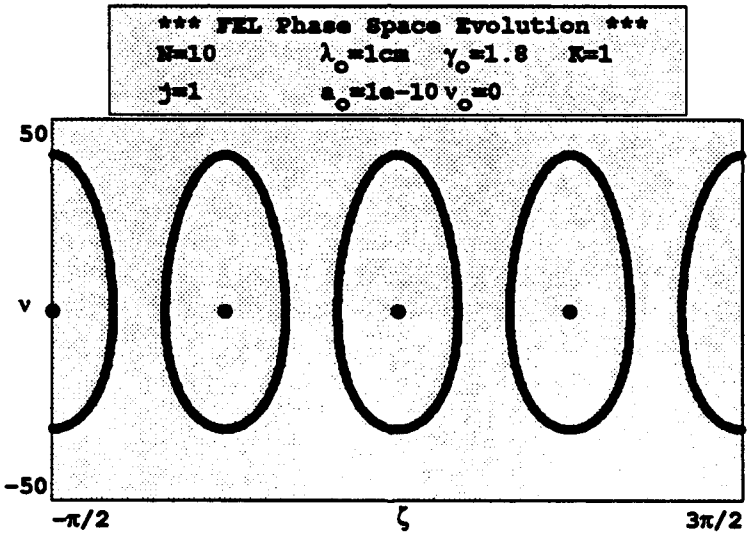

Figure 13. Phase-space orbits without light in large K/γ regime.

Given that the analytical difficulties cannot be resolved, the range of validity for the Bessel function coupling coefficient can be evaluated by comparison with simulations. The region of large K/γ is the most likely regime for discrepancy. Figure 14 shows the phase-space evolution with light in the high K/γ regime. Not

only do the orbits take on a different shape, but the electrons appear to travel further along their orbits than before. An unexpected benefit of such motion is improved gain compared to the low K/γ model using the pendulum equation. Since the pendulum equation model has no dependence on K/γ, it is immediately apparent that the two models disagree. The disagreement cannot be resolved by replacing the Bessel function coupling coefficient with some more accurate functional form, which was the original aim of this research. A more fundamental problem lies in the pendulum equation description.

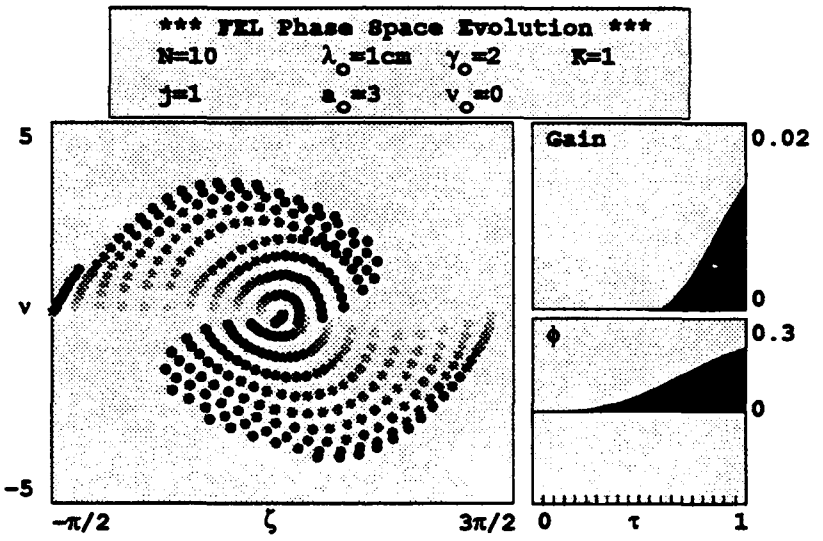

Figure 14. Exact averaged phase-space trajectories for the linearly-polarized undulator in the large K/γ regime.

In order to fully understand what happens, it is necessary to return to the helical undulator. Theoretically, this model has none of the complications that plague the linear case. The helical case can be solved exactly with only the assumption of low gain, just as (33) was derived. The result is

$$\frac{\dot{\beta}_z}{1-\beta_z^2} = \frac{AK[\omega_o+\omega(1-\beta_z)]\cos[(k+k_o)z-\omega t+\phi]}{1+K^2+A^2-2AK\sin[(k+k_o)z-\omega t+\phi]} \quad . \tag{41}$$

This result can be solved numerically, transformed directly into phase-space variables and displayed as in the linear case. The complication of averaging is unnecessary. Figure 15 shows a large K/γ case in a helical undulator. This, too, does not agree with the pendulum equation, shown in Figure 12, which is independent of γ. The assumptions, $K/\gamma \ll 1$ and γ = constant, used to derive the pendulum equation do not apply in this regime, and the pendulum equation is not the appropriate description.

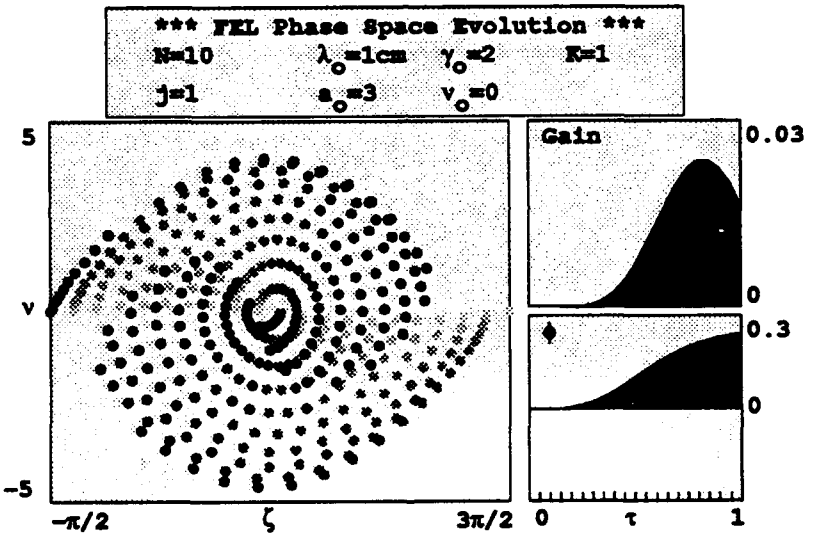

Figure 15. Phase-space trajectories in a helical undulator in the large K/γ regime.

The result that the pendulum equation itself doesn't apply in the large K/γ regime supports the contention that an analytical result for all regimes is an impossible goal. The validity of the Bessel function coupling coefficient doesn't

extend into this regime, not because it is an inaccurate functional form, but because there is no appropriate coupling coefficient concept. That would require the same basic equation, but with a different constant multiplicative factor. The basic equation itself is inadequate.

If the value of K/γ is chosen such that the pendulum equation model is an accurate description for the helical case, the accuracy of the linear model with the Bessel function coupling coefficient can be evaluated. By exploration with different parameters, $K/\gamma \approx 1/4$ is the limit of validity for the pendulum equation in the helical case. With identical parameters, the linear model is compared to the pendulum equation with the Bessel function coupling coefficient. In Figure 16, the result for the limiting case can be seen. The Bessel function coupling coefficient accurately compares with the exact solution. This leads to a surprising conclusion: The Bessel function coupling coefficient is accurate in all regimes of K/γ where the pendulum equation itself can be said to apply. The conditions required to make the assumptions invalid, also change the basic physics involved. If a restriction is made to regimes where the pendulum equation can be used, then the Bessel function coupling coefficient compares extremely well with the exact solution. Outside this regime, then a more fundamental equation like (33) or (41) must be used instead of the pendulum equation.

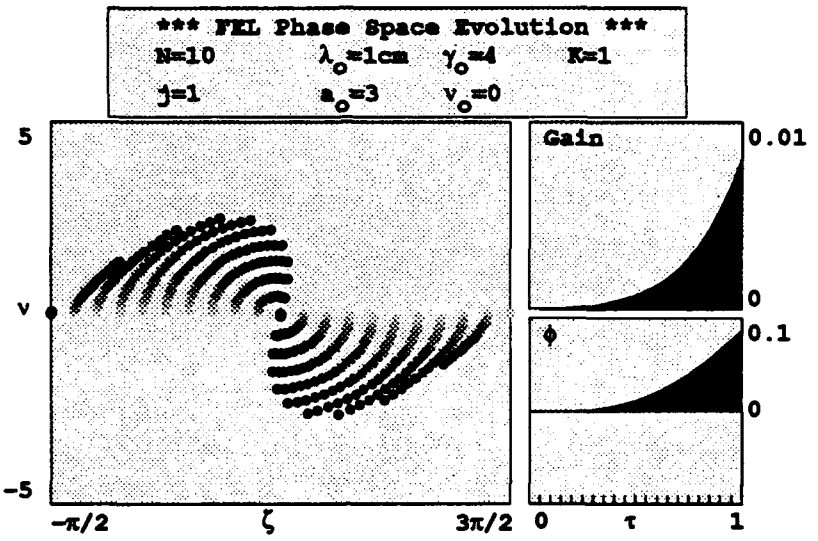

Figure 16. Exact averaged phase-space trajectories in the linearly-polarized undulator at the limit of validity for the pendulum equation.

IV. EVALUATING FEL PERFORMANCE FROM ACCELERATOR SIMULATIONS

A. ACCELERATOR SIMULATIONS

While accelerator technology and simulation is highly advanced, integration of this technology with FEL technology has often lagged behind. This is partly because there is no concise means of describing what the effect of beam design will be on a specific FEL design. A recent trend has been to develop integrated computer models that incorporate both accelerator simulation and FEL simulations. The INEX code at Los Alamos National Lab (LANL) was designed to integrate PARMELA accelerator and FELEX free electron laser codes. This accomplishment can accurately model the entire FEL system from beam creation at the cathode to the laser output. The price of this achievement has been complexity. Both PARMELA and FELEX require a vast amount of input to specify all the components. The INEX code is difficult to run, takes a long time on a CRAY computer, and produces voluminous output. This is painstaking and costly which makes it of value only in the characterization of mature designs. In practice, accelerator and FEL designs are pursued independently. Beam quality requirements are usually specified only vaguely, and are often at the limit of current technology.

A simple code is developed for use with the accelerator simulation. It allows quick, and easy interpretation of the beam's performance as an FEL. There is a sacrifice of accuracy, but it is of improved use as a tool for the designer, who can test an accelerator design on specific FEL designs. This is an improvement over vague beam quality specifications which are independent of specific FEL parameters.

B. BEAM QUALITY EFFECTS ON UNDULATOR TRAJECTORIES

As was seen in the preceding chapter, the motion of individual electrons inside the undulator can be solved by approximate analytical and exact numerical means. The exact trajectory of an individual electron can be determined by its initial conditions. This leads to the important premise that beam quality manifests itself as a spread in initial conditions. The final exit conditions from the accelerator simulation are the initial conditions for the FEL undulator. Therefore, the six phase-space coordinates of each of the sample electrons provides the data base for beam quality predictions. For N_e electrons, there will be $6N_e$ coordinates. Typical simulations use up to 20,000 sample electrons, and deal with 120,000 coordinates.

An accepted measure of beam quality from the accelerator community is emittance. It has several definitions and has been the source of confusion in many instances. Emittance, as it will be used throughout this chapter, is defined as the transverse rms emittance [Ref. 24]

$$\varepsilon_{rms} = 4\left[\langle x^2\rangle\langle x'^2\rangle - \langle xx'\rangle^2\right]^{1/2} \tag{42}$$

where x is a coordinate, and $x' = dx/dz$. The $\langle\ \rangle$ denotes an average value over the sample electrons. For extremely relativistic beams, x' corresponds to an angle with the longitudinal axis, $\theta_x = \beta_x/\beta_z$. The transverse emittance has two components, ε_x and ε_y, each defined by (42). The combined transverse emittance can be found as $\varepsilon_{trans} = \sqrt{\varepsilon_x \varepsilon_y}$. High energies make this number lower due to relativistic effects, so a normalized emittance can be defined by $\varepsilon_{norm} = \gamma\varepsilon$. This will be explicitly stated when used. Another characterization of emittance is the area enclosed by an ellipse in phase-space that contains a certain percentage of the sample electrons. An example is the "90%" emittance, $\varepsilon_{90\%}$ [Ref. 25], which is the area of the ellipse which encloses 90% of the sample electrons. In practice, the 90% emittance is easier to measure than ε_{rms}. They are related but depend on the

specifics of the distributions to be quantitatively related [Ref. 26].

The effect of initial conditions on trajectories in the undulator can be found by approximate analytical results. First, introduce the additional complication of non-ideal fields. This is included because it is a common feature, especially in linearly-polarized undulators. The magnetic field of the undulator can be represented by

$$\vec{B} = B[\ 0,\ \sin(k_o z)\cosh(k_o y),\ \cos(k_o z)\sinh(k_o y)] \quad , \tag{43}$$

where $k_o = 2\pi/\lambda_o$ is the undulator wave number, and λ_o is the undulator period [13]. This assumption correctly accounts for off-axis fields, with their increasing magnitude towards the magnetic pole pieces. This is also more realistic than (17), because it is a solution to the Maxwell equations for a static field whereas (17) was not. Sometimes the pole pieces are shaped to provide a similar field structure in the other transverse direction because of the desirable focusing properties [Ref. 14]. This is called two-plane focusing, but will be ignored here. It is a minor matter, however, to add it to the resulting code.

The motion of the electrons can be found in a similar manner as the previous chapter. The effect of beam quality can be found by examining the electron trajectories without significant effect from light. The wavelength of light will be assumed to be defined by the resonance condition, so that the motion can be discussed with respect to the meaningful phase-space coordinates introduced earlier, (ζ,v). The Lorentz force equation gives the following component equations

$$\dot{\beta}_x = \frac{-eB}{\gamma mc^2}[\ \cos(k_o z)\dot{y}\sinh(k_o y) - \dot{z}\sin(k_o)\cosh(k_o y)] \quad , \tag{44a}$$

$$\dot{\beta}_y = \frac{eB}{\gamma mc^2}\dot{x}\cos(k_o z)\sinh(k_o y) \quad , \quad \text{and} \tag{44b}$$

$$\dot{\beta}_z = \frac{-eB}{\gamma mc^2}\dot{x}\sin(k_o z)\cosh(k_o y) \quad . \tag{44c}$$

The x component is a perfect derivative and can be integrated immediately

$$\beta_x(y,z) = \beta_x(0) + \sqrt{2}\frac{K}{\gamma}\cosh(k_o y)[1-\cos(k_o z)] \quad ,$$

where $K = eB\lambda_o/2\pi mc^2$, and $\beta_x(0)$ is the β_x at $z = 0$. For nearly perfect injection, there is little correction from treating $\beta_x(0) \approx \sqrt{2}K/\gamma$. Therefore, the x component can be written as

$$\beta_x = -\sqrt{2}\frac{K}{\gamma}\cosh(k_o y)\cos(k_o z) \quad . \tag{45}$$

Substituting (45) into (44b) gives

$$\dot{\beta}_y = -2ck_o\frac{K^2}{\gamma^2}\cos^2(k_o z)\sinh(2k_o y) \quad .$$

The fast oscillating motion in the $\cos(k_o z)$ term is uninteresting so it is more useful to take the average motion over several periods of the undulator. The averaged equation is

$$\dot{\bar{\beta}}_y \frac{1}{\lambda_o}\int_0^{\lambda_o}\dot{\beta}_y dz = -\frac{cK^2k_o}{2\gamma^2}\sinh(2k_o y) \quad .$$

For small deflections from the z-axis, use the small angle approximation $\sinh(2k_o y) \approx 2k_o y$, so that

$$\ddot{y} = -\frac{c^2K^2k_o}{2\gamma^2}y \quad .$$

This describes simple harmonic motion in the y-z plane which is called betatron motion. Using the variable $\tau = ct/L$, this can be rewritten in dimensionless form

$$\overset{oo}{y}(\tau) = -\omega_\beta^2 y(\tau) \quad , \tag{46}$$

where the open circles denote derivative with respect to τ, and $\omega_\beta = 2\pi NK/\gamma$ is the dimensionless betatron frequency.

The exact betatron motion is determined by the initial conditions. The solution for the y-component is

$$y(\tau) \approx y_o \cos(\omega_\beta \tau) + \frac{L\theta_y}{\omega_\beta} \sin(\omega_\beta \tau) \quad , \tag{47}$$

where y_o is the initial y position, L is the undulator length, and θ_y is the initial angle with respect to the z axis [Ref. 17]. The betatron motion causes a periodic deflection in the undulator similar to the periodic deflection in the x direction but with much longer period. Because the motion is coupled by conservation of energy through $\gamma^{-2} = 1 - \beta_x^2 - \beta_y^2 - \beta_z^2$, the deflection in the y direction causes changes in β_z. Changes in the x position have no effect without two-plane focusing. A change in the angle θ_x adds a constant value to β_x. The approximate average z motion is

$$\bar{\beta}_z \approx 1 - \frac{1}{2}\gamma^{-2}(1+K^2) - \frac{1}{2}\omega_\beta^2 \frac{y_o^2}{L^2} - \frac{1}{2}\theta^2 \quad , \tag{48}$$

where $\theta^2 = \theta_x^2 + \theta_y^2$. The effect on ν can be computed from the definition $\nabla = L[(k+k_o)\bar{\beta}_z - k]$. If this definition is taken as a transformation then for each sample electron there will be an associated phase velocity given by

$$\nu_j = L(k+k_o)\left[1 - \frac{(1+K^2)}{2\gamma^2} - \frac{1}{2}\omega_\beta^2 \frac{y_j^2}{L^2} - \frac{\theta_j^2}{2} - \frac{k}{(k+k_o)}\right] \quad , \tag{49}$$

where j denotes the coordinates of the j^{th} electron. The real resonance condition is defined by

$$\nu_{res} = \frac{1}{N_e}\sum_0^{N_e} \nu_j = 0 \quad . \tag{50}$$

This can be satisfied by a unique value of k which corresponds to the resonant optical wavelength for this electron beam.

Now, a complete, dimensionless description can be made which expresses the effect of initial conditions on the phase velocity using (49). A sampling of electrons can be used to make a distribution plot of phase velocity, which in turn can be used as a diagnostic for FEL performance.

C. PHASE VELOCITY DISTRIBUTIONS FROM INITIAL CONDITIONS

Using equation (49) as a formula for computing the effect of initial conditions on the phase velocity, each electron can be assigned a value, ν_j, as a function of its six phase space coordinates. This can be made into a distribution for each slippage distance, the distance that light moves ahead of the electrons, since that is the relevant interaction length in the micropulse. However, there may be thousands of slippage lengths in a long micropulse with a short optical wavelength, thereby making the number of plots prohibitive. A short characterization of each slippage length may be given by the centroid and rms width of each distribution. If the basic shape of the individual distributions are roughly the same, then this will be a useful simplification.

Figure 17 shows a typical slippage-length phase-velocity distribution. The resonance parameter refers to ν. Since exact resonance is defined by $\nu = 0$, this is effectively a plot of $\Delta\nu$. The sample electrons came from the PARMELA simulation of an accelerator design for a compact FEL under development at LANL. Beam parameters are: peak current, $I = 400$A; beam energy, $\gamma mc^2 = 15$MeV; and pulse length, $\Delta t = 16$ps. The FEL parameters are: undulator period, $\lambda_o = 0.9$cm; number of periods, $N = 15$; and undulator parameter, $K = 0.7$. The resonance condition, (50), gives an optical wavelength of 0.7μm. Beam quality was on the average $\varepsilon = 10\pi$ mm-mrad, and energy spread $\Delta\gamma/\gamma = 0.07\%$.

The shape of Figure 17 is highly asymmetric. This can be understood in terms of dividing the effects into two broad categories: transverse position and angle, and real energy spread. Any combination of initial transverse phase space coordinates will translate into a reduction in the phase velocity. Specifically, the resulting betatron oscillation constitutes a reduction in the parallel component of velocity, and therefore results in a reduction of the phase velocity. Real energy spread may, or may not, have a well defined shape. Most typically, whatever effects that result from unequal acceleration tend to be symmetric. Therefore, a

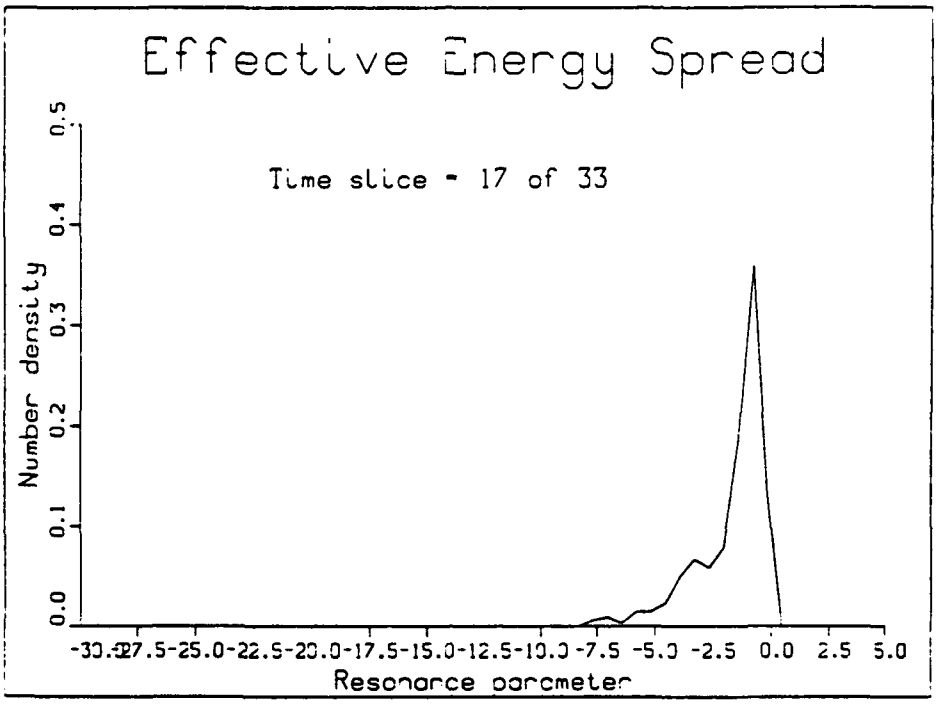

Figure 17. Phase velocity distribution in one slippage distance.

beam dominated by real energy spread would have a more, or less symmetric distribution while a beam dominated by angular divergence would show pronounced inhomogeneous broadening. An approximation to the distribution due solely to angular divergence is a straight exponential $e^{-\nu/\sigma}$. The beam in Figure 17 is an example of a case dominated by angular divergence. For the beam used, the real energy spread is $\Delta\gamma/\gamma = 0.07\%$, and the transverse rms emittance is $\varepsilon = 10\pi$ mm-mrad. Without specific FEL parameters, these quantities alone cannot be interpreted usefully.

Figure 18 shows the rms width of the distribution in each slippage distance as a function of the position along the micropulse. In the center of the micropulse, the value remains essentially steady at $\Delta\nu = 2.0$. This value must be compared to the relevant small-signal gain bandwidth, $\Delta\nu = \pi$, as shown in Figure 5. This distribution would fall entirely within the gain bandwidth, and therefore, one

would not expect any serious gain degradation. This is not the only comparison that can be made. It is also possible to take the resulting distributions and use them with the theories of beam quality effects. Namely, it is a simple extension to take the results and apply them to the theory of Blau and Colson and find a characteristic function that can be used in the "integral equation" [Ref. 27]. Since this area has already been well explored, it is useful to take advantage of the previous work as much as possible. The phase velocity distributions provide the bridge to this useful area.

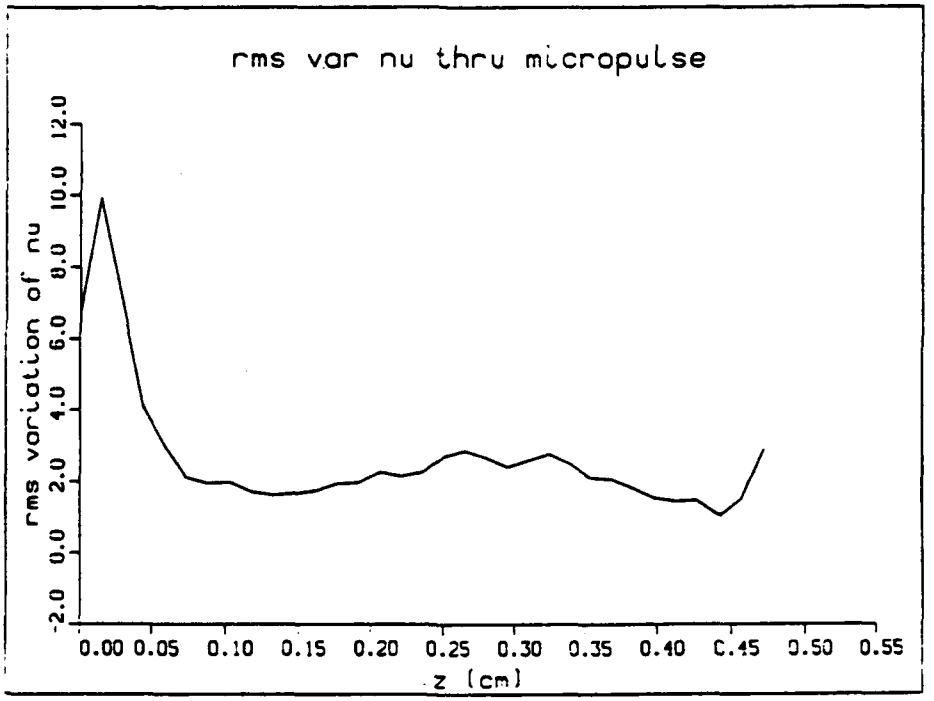

Figure 18. Phase velocity distribution rms variation as a function of position along the micropulse.

The shape of figure 18 also shows a dramatic drop in beam quality at the end of the micropulse. However, trends in this data must be compared to the particle density. Large variations at the ends are mitigated by the relatively low currents there. Figure 19 shows how particle density varies along the micropulse. The ends have relatively low current, and therefore, temper the effects of beam quality there.

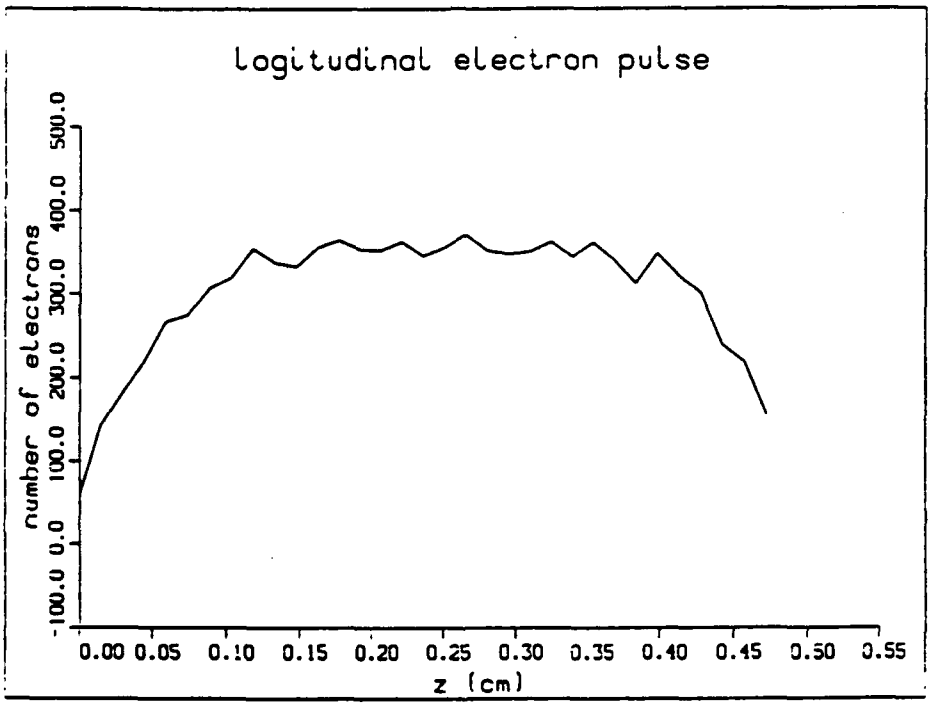

Figure 19. Particle density as a function of position in the micropulse.

The way phase-space coordinates are manipulated by accelerator beam-line components and focusing elements can dramatically affect FEL performance even though the inherent beam quality remains the same. Liouville's theorem guarantees that the six-dimensional phase-space hypervolume will remain constant for conservative forces [Refs. 21,25]. Because the beam is highly relativistic, only the transverse phase-space distribution can change. Liouville's theorem then predicts that the transverse emittance is a constant of motion. Although the emittance is constant, different combinations of the phase-space coordinates do not

guarantee the same effect in the FEL. It has been shown that transverse phase-space coordinates must be "matched" to achieve the best performance for a given inherent beam quality. The matching condition [Ref. 26] is

$$\langle y^2 \rangle = \frac{\varepsilon L}{2\pi\omega_\beta} \quad . \tag{51}$$

While this can be done for any small fraction of the micropulse, it cannot be achieved for the entire beam simultaneously. Some middle ground must be chosen to hopefully achieve optimum FEL performance.

This also points out the inaccuracy of using a single transverse emittance value for the entire pulse. If we look at the transverse emittance at any one slippage length, it remains at a relatively steady value, consistent with Liouville's theorem. However, the actual phase space plots may be distributed in radically different ways. Although the plots take up the same area, an ellipse enclosing a majority of the points can be highly eccentric. Since emittance measures only the area, a matched ellipse by (51) has the same emittance as a highly eccentric ellipse, although the later doesn't satisfy (51). The unmatched section may oscillate on the whole, whereas the matched section is balanced and remains in the same distribution throughout. Transverse emittance as a function of longitudinal position in the micropulse is shown in Figure 20, and provides no information about how the individual sections are matched. If all the slippage lengths are projected onto the same plot, the resulting emittance may be much greater than any individual slice. This is because there may be large areas of non-overlapping coverage that together enclose a larger area than any one slice. A single number that measures the transverse emittance of the beam cannot account for any of these effects, nor does the plot of emittance as a function of position in the micropulse. The only way to incorporate all of these considerations is to examine the phase velocity distribution functions at each slice, or more simply a plot of the rms width of these distributions as a function of position.

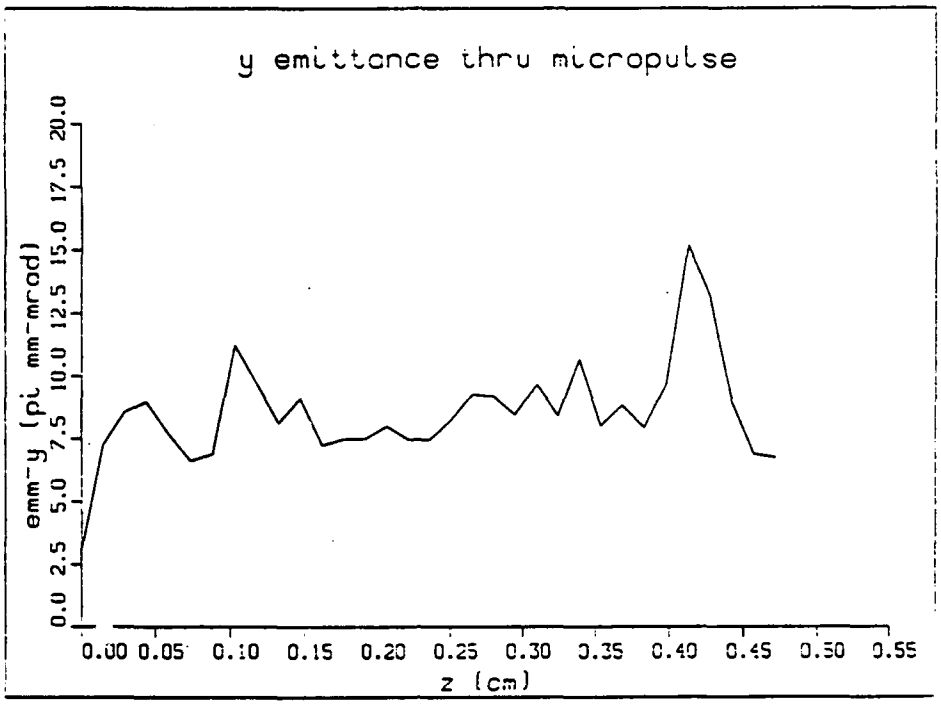

Figure 20. Transverse emittance as a function of position in the micropulse.

In addition to the rms width of the distributions, the maximum or centroid of the distribution may vary from slippage distance to slippage distance. Figure 21 illustrates the result obtained from the accelerator design under review. Again, there is a strong variation at the ends. The same argument presented previously applies to the extreme variation at the ends. However, there may be a systematic variation along the entire length of the micropulse. In systems where the slippage length is short compared to the micropulse, this may manifest itself as a temporal frequency variation in the optical pulse. However, this effect is not limited to a frequency "chirp," but the details of how this works in short pulse, long slippage distance systems which account for collective effects has not yet been addressed.

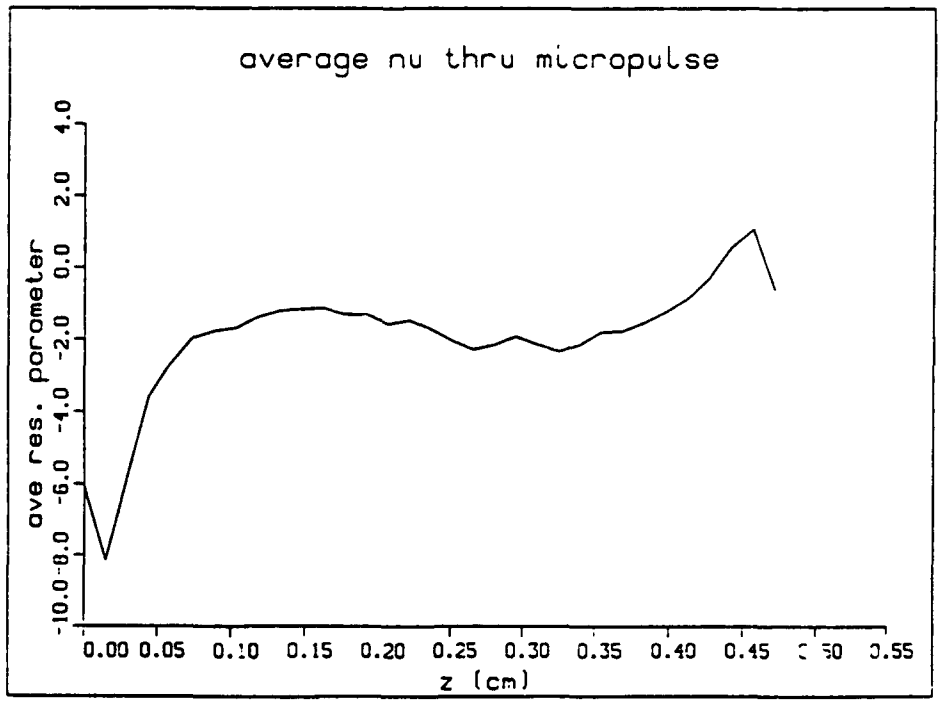

Figure 21. Variation of phase velocity along micropulse.

In summary, the six phase-space coordinates of all the sample electrons can be put into a nominal number of plots that describe much of the essential FEL physics. The particle density show what weight to give the various effects. The average phase velocity describes any systematic variation in the frequency in the optical pulse, but slippage length communication must be considered. The width of the phase velocity distribution along the micropulse most clearly illustrates the beam quality effects, and can be used with any number of well established theories. Various standard quantities can be computed for comparison to the more frequently available measurements, for example, those obtained by experiment. And finally, this program can easily recommend values for beam matching parameters.

LIST OF REFERENCES

1. J. M. J. Madey, J. Appl. Physics. **42**, 1906 (1971).
2. L. R. Elias, W. M. Fairbank, J. M. J. Madey, G. J. Schwettman, T. I. Smith, Phys. Rev. Lett. **36**, 717 (1976).
3. D. A. G. Deacon, L. R. Elias, J. M. J. Madey, G. J. Ramian, H. A. Schwettman and T.I. Smith, Phys. Rev. Lett. **38**, 892 (1977).
4. W. B. Colson, Phys. Lett. **64A** , 190 (1977).
5. W. B. Colson and S. K. Ride, Phys. Lett. **76A** , 379 (1980).
6. W. B. Colson , IEEE J. Quantum Electronics **QE-17(8)** 1417 (1981).
7. J. M. J. Madey and R. C. Taber in: Physics of Quantum Electronics, vol. 7, eds., Jacobs et al. , Addison-Wesley, Reading, MA, (1980).
8. W. B. Colson. G Dattoli, and F. Ciocci, Phys. Rev. **A31** , 828 (1985).
9. B. W. J. McNeil and W. J. Firth, IEEE J. Quantum Electronics **QE-21 (7)** 1031 (1985).
10. B. W. J. McNeil and W. J. Firth, Nucl. Instr. and Meth. **A259** , 240 (1987).
11. B. W. J. McNeil and J. W. Firth, Nucl. Instr. and Meth. **A272** 275 (1988).
12. C. J. Elliott and M. J. Schmitt, Nucl. Instr. and Meth. **A250** 432 (1986).
13. J. P. Blewett and R. Chasman, J. Appl. Phys. **48**, 2692 (1977).
14. C. J. Elliott and M. J. Schmitt, Nucl. Instr. and Meth. **A259** , 177 (1987).
15. E. T. Scharlemann, J. Appl. Phys. **58**, 2154 (1985).
16. J. D. Jackson, *Classical Electrodynamics* , Wiley, New York, (1975).
17. W. B. Colson, "Classical Free Electron Laser Theory", Chapter 5 in "*Free Electron Laser Handbook*", W. B. Colson, C. Pellegrini and A. Renieri (*editors*), North-Holland Physics, Elsevier Science Publishing Co., Inc., The Netherlands (1990).

18. H. Kogelnik and T. Li, Proceedings of the IEEE, **54**, 1312 (1966).

19. K. Halbach, *Bendor Free Electron Laser Conference*, eds. M. Billardon and D. A. G. Deacon, Journal de Physique, Colloque **C1-44**, p. 211 (1983)

20. W. B. Colson, *Free Electron Laser Theory*, Ph.D. thesis at Stanford University, 1977.

21. R. Z. Sagdeev, D. A. Usikov, and G. M. Zaslavsky, *Nonlinear Physics*, Harwood academic Publishers, Switzerland (1988).

22. W. E. Boyce and R. C. DiPrima, *Elementary Differential Equations*, Wiley, New York, (1977).

23. I. S. Gradshteyn and I. M. Ryzhik, *Table of Integrals, Series, and Products* , Academic Press, San Diego, (1980).

24. Lapostolle, P., IEEE Trans, Nucl. Sci. **18**, 1101 (1971a).

25. C. LeJeune and J. Aubert, "Emittance and Brightness: Definitions and Measurements," in *Applied Charged Particle Optics*, Ed., A. Septier, Advances in Electronics and Electron Phys., Supp. 13A (1980).

26. J. C. Goldstein, B. E. Newnam, R. K. Cooper, and J. C. Comly, Jr. in *Laser Techniques in the Extreme Ultraviolet*, AIP Conf. Proc. No.**119**, p.293, eds. S. E. Harris and T. B. Lucatorto, American Institute of Physics, N. Y., (1984).

27. W. B. Colson and J. Blau, Nucl. Instr. & Methods in Phys. Res. **A259**, 198 (1987).

INITIAL DISTRIBUTION LIST

1.	Defense Technical Information Center Cameron Station Alexandria, Virginia 22304-6145	2
2.	Library, Code 52 Naval Postgraduate School Monterey, California 93943-5002	2
3.	Professor William B. Colson, Code PH/Cw Department of Physics Naval Postgraduate School Monterey, California 93943-5000	9
4.	Professor Xavier K. Maruyama, Code PH/Mx Department of Physics Naval Postgraduate School Monterey, California 93943-5000	1
5.	Professor K. E. Woehler Code PH/Wh Chairman, Department of Physics Naval Postgraduate School Monterey, California 93943-5000	1